(NASA-CR-172142) EVALUATION OF NON-INTRUSIVE FLOW MEASUREMENT TECHNIQUES FOR A RE-ENTRY FLIGHT EXPERIMENT Final Report, 26 Jan. 1982 - 25 Jan. 1983 (Princeton Resources, Inc., N. J.) 97 p G3/15

N84-13212

Unclas 42595

NASA Contractor Report 172142

EVALUATION OF NON-INTRUSIVE FLOW MEASUREMENT TECHNIQUES FOR A RE-ENTRY FLIGHT EXPERIMENT

R. B. MILES, D. A. SANTAVICCA, AND M. ZIMMERMANN
Princeton University
Princeton, New Jersey 08544

Cooperative Agreement NCCI-64

NOVEMBER 1983

National Aeronautics and Space Administration

Langley Research Center
Hampton, Virginia 23665

TABLE OF CONTENTS

LIST OF SYMBOLS

Symbol	Units	Description
A_{jk}	$second^{-1}$	Einstein spontaneous emission coefficient for level j to level k
C_i		concentration of species i
c	meters/second	speed of light in vacuum
D	meters	laser beam diameter between $1/e^2$ intensity points
d	meters	thickness of radiating layer
E_j	joules	energy of the j^{th} energy level
F		f number of collection optics (lens focal length/lens diameter)
g_j		degeneracy of the j^{th} energy level
h	6.6256×10^{-34} joule-second	Planck's constant
$\hbar$	1.0545×10^{-34} joule-second	Planck's constant/2π
I_{AS}	$watts/meter^2$	intensity of coherent anti-Stokes Raman signal
I_P	$watts/meter^2$	intensity of pump laser
I_S	$watts/meter^2$	intensity of probe (Stokes) laser
I_{jk}	$watts/meter^2$	emission intensity from level j to level k
I_o	$watts/meter^2$	blackbody radiation intensity per unit wavelength
I_λ	$watts/meter^2$	emission intensity per unit wavelength
J''		lower rotational state
J_λ		emission coefficient per unit wavelength
Δj		fractional population difference between transition levels
K_λ		absorption coefficient per unit wavelength

Symbol	Units	Description
K'_λ		absorption coefficient per unit wavelength
k	1.38054×10^{-23} joules/°K	Boltzmann's constant
$\hat{k}$		unit vector in the direction of laser propagation
L	meters	sample volume length
ℓ	meters	length of the laser Doppler velocimeter fringe region
M		Mach number
M_∞		free stream Mach number
m	Kg	mass
N	$meters^{-3}$	total species number density
N_i	$meters^{-3}$	number density of species i
n(m)	meters	distance outward from windward centerline of the shuttle
n_p		number of pulses per measurement interval
P_{AS}	watts	coherent anti-Stokes signal power
P_{RAMAN}	watts	Raman scattered signal power
$P_{RAYLEIGH}$	watts	Rayleigh scattered signal power
P_S	watts	power of probe (Stokes) laser
P_o	watts	incident power of the laser
Q_i	$meters^2$/ steradian-molecule	Rayleigh cross section of species i
Q_{ij}	$meters^2$	quenching collision cross section of species i with species j
q(v',v'')		Franck-Condon factor between levels v' and v''
R_N	meters	equivalent nose radius of space shuttle
S	meters	distance from the space shuttle nose
S/N		signal to noise ratio

Symbol	Units	Description
$(S/N)_{CARS}$		signal to noise ratio for coherent anti-Stokes Raman scattering
$(S/N)_{RAMAN}$		Raman scattering signal to noise ratio
$(S/N)_{RAYLEIGH}$		Rayleigh scattering signal to noise ratio
s'	meters	displacement along a ray of light
T	°K	temperature
T_w	°K	wall temperature of shuttle
Δt	sec	laser pulse duration
U	meters/second	flow velocity
$\vec{U}$	meters/second	flow velocity vector
U_l	meters/second	particle velocity
U_∞	km/second	free stream velocity
$\bar{u}$	meters/second	relative velocity
v	km/second	velocity
v'		upper vibrational states
v''		lower vibrational states
$\bar{v}_{ij}$	meters/second	relative velocity between species i and j
w	meters	width of laser doppler velocimetry fringe region
x_f	meters	distance between interference fringes
z	meters	interaction length
α	degrees	angle of attack
β	degrees	intersection angle of lasers for laser Doppler velocimetry
γ	radians/second	Raman line width
η		combined collection and detection efficiency

Symbol	Units	Description
η_C		efficiency of the collection optics
η_D		efficiency of the detector
θ	degrees	half body angle
λ	meters	wavelength
$\Delta\lambda$	meters	width of spectral filter in wavelength
λ_{AS}	meters	anti-Stokes wavelength
λ_P	meters	pump laser wavelength
λ_S	meters	probe (Stokes) laser wavelength
λ_{jk}	meters	emission wavelength for transition from level j to level k
λ_o	meters	laser wavelength
λ_{21}	meters	absorption wavelength of the particular species
ν	Hertz	radiation frequency
$\Delta\nu$	Hertz	spectral linewidth--full width at half maximum
ν_B	Hertz	beat frequency produced by particle passing through the fringe pattern in laser Doppler velocimetry
$\delta\nu_D$	Hertz	Doppler shift of resonant frequency
$\Delta\nu_G$	Hertz	thermal (Gaussian) spectral linewidth--full width at half maximum
$\Delta\nu_L$	Hertz	Lorentzian spectral linewidth--full width at half maximum
ν_o	Hertz	absorption frequency
$\Delta\nu_o$	Hertz	free spectral range of the Fabry-Perot interferometer
ρ	Kg/meters^3	density
ρ_∞	Kg/meters^3	free stream density

Symbol	Units	Description
σ	meters^2	collision cross section
$(\frac{d\sigma}{d\Omega})_{RAMAN}$	meters^2/ steradian-molecule	differential Raman scattering cross section
τ		optical length
χ	meters^3/joule	nonlinear susceptibility
χ_{NR}	meters^3/joule	non-resonant part of the nonlinear susceptibility
χ_R	meters^3/joule	resonant part of the nonlinear susceptibility
Ω_c	steradians	solid angle of the collection optics
$\Delta\omega$	radians/second	Raman transition frequency
ω_{AS}	radians/second	coherent anti-Stokes frequency
ω_P	radians/second	pump laser frequency
ω_S	radians/second	probe (Stokes) laser frequency

LIST OF FIGURES

LIST OF TABLES

EVALUATION OF NON-INTRUSIVE FLOW MEASUREMENT TECHNIQUES FOR A RE-ENTRY FLIGHT EXPERIMENT

R. B. Miles, D. A. Santavicca, and M. Zimmermann

Abstract

This study evaluates various non-intrusive techniques for the measurement of the flow field on the windward side of the Space Shuttle orbiter or a similar re-entry vehicle. Included are linear (Rayleigh, Raman, Mie, Laser Doppler Velocimetry, Resonant Doppler Velocimetry) and nonlinear (Coherent Anti-Stoeks Raman, Laser-Induced Fluorescence) light scattering, electron-beam fluorescence, thermal emission, and mass spectrometry. Flow-field properties were taken from a nonequilibrium flow model by Shinn, Moss, and Simmonds at the NASA Langley Research Center. Conclusions are, when possible, based on quantitative scaling of known laboratory results to the conditions projected. Detailed discussion with researchers in the field contributed further to these conclusions and provided valuable insights regarding the experimental feasibility of each of the techniques.

EVALUATION OF NON-INTRUSIVE FLOW MEASUREMENT TECHNIQUES FOR A RE-ENTRY FLIGHT EXPERIMENT

1. Introduction

This project was undertaken to determine which, if any, of a variety of non-intrusive diagnostic techniques might be useful in determining flow properties on the windward side of a re-entering Space Shuttle orbiter or a separate re-entry vehicle. The procedure was to first estimate the detection capabilities of the techniques at conditions corresponding to those expected in the flow field surrounding the Space Shuttle orbiter or other re-entry vehicle as it passes between 80 and 40 km in altitude. Where possible we used existing experimental results and extrapolated to the desired conditions. In some of these estimates, we were guided by ongoing work in our own laboratories and in others by results published in the literature. Subsequently, a presentation was made to the Princeton Advisory Group which discussed the relative merits of each techniques plus a list of the important parameters to be measured. In order to further explore the promises and limitations of each of the techniques, a wide variety of researchers were visited and detailed discussions undertaken. These included trips to NASA Langley, United Technologies, NASA Ames, University of California-Berkeley, Sandia-Livermore Laboratories, and Stanford University. This provided an opportunity to obtain specific comments and perceptions from these researchers with regard to the state-of-the-art and the potential of each of the techniques. Many of these comments are included in the appendices in which the techniques are discussed in detail.

2. Summary of the Results

The flow-field conditions which were used in this study were largely taken from work conducted at NASA Langley by J. L. Shinn, J. N. Moss, and A. L. Simmonds.[1] Figure 1 is a sketch showing the equivalent hyperboloid and coordinates used for that study. Figures 2 and 3 show plots of velocity, density, and temperature for a re-entering Shuttle orbiter at altitudes of 74.95 km and 52.43 km, respectively. Each is shown as a function of the distance from the wind-ward surface at two points along the centerline. Here, the calculation was made for an equivalent hyperboloid whose parameters are determined by the angle of attack of the re-entering vehicle. The arrows indicate the conditions at the wall assuming a finite catalytic wall material. The free-stream conditions and equivalent-body parameters are given in Table 1.[2] Each of the curves in Figure 2 and 3 terminates at the shock boundary, and thereafter the free-stream conditions apply.

These calculated results depend strongly on the effects of nonequilibrium gas phase chemistry and surface catalytic activity. Figures 4 and 5 show calculated values of species mass fractions at 75 km altitude assuming in Figure 4 a non-catalytic wall and in Figure 5 a fully or equilibrium catalytic wall. Depending on the range in catalytic activity, the wall temperature can vary by as much as 30%. Comparisons of species concentrations calculated for a catalytic or non-catalytic wall are apparent. For, example, a large change in the O_2 species concentration near the wall indicates strong catalytic effects. At low altitudes and lower speeds the temperature behind the shock is too low to produce significant radical concentrations (Figure 6).[3] The calculated values of species concentrations and temperature distributions behind the shock depend on reaction rates and flow-field calculation methods. Consequently, the validity of the model

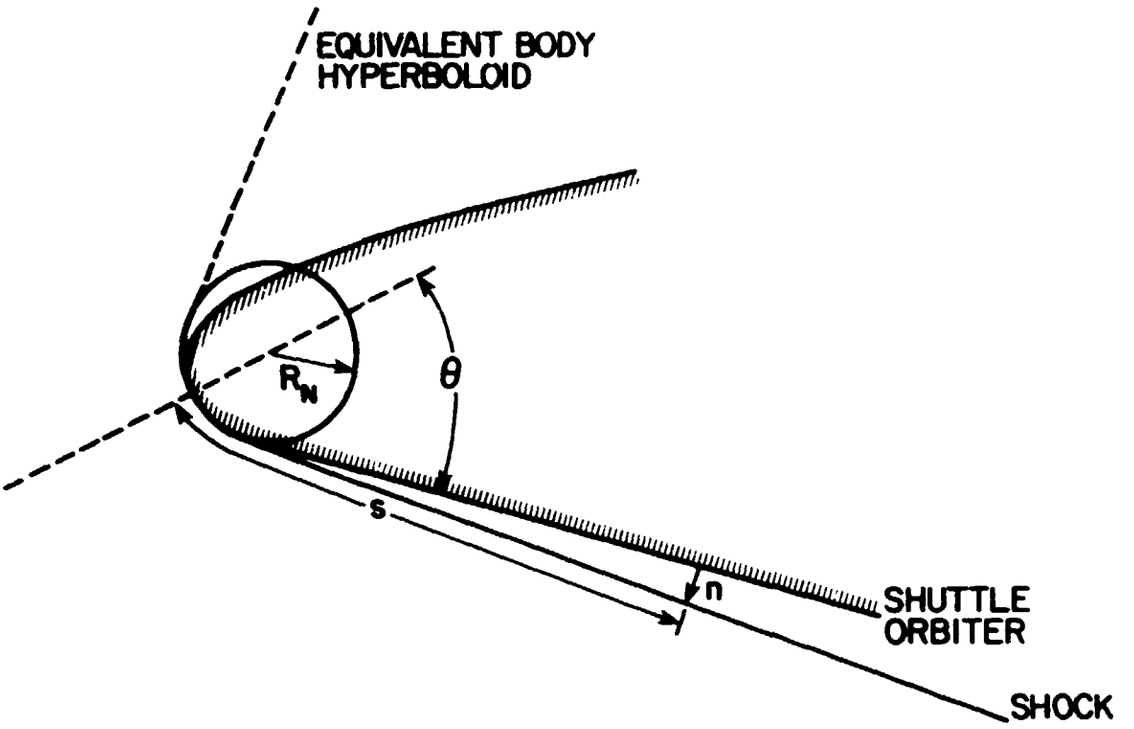

Figure 1. Coordinates for calculation of flow field conditions.

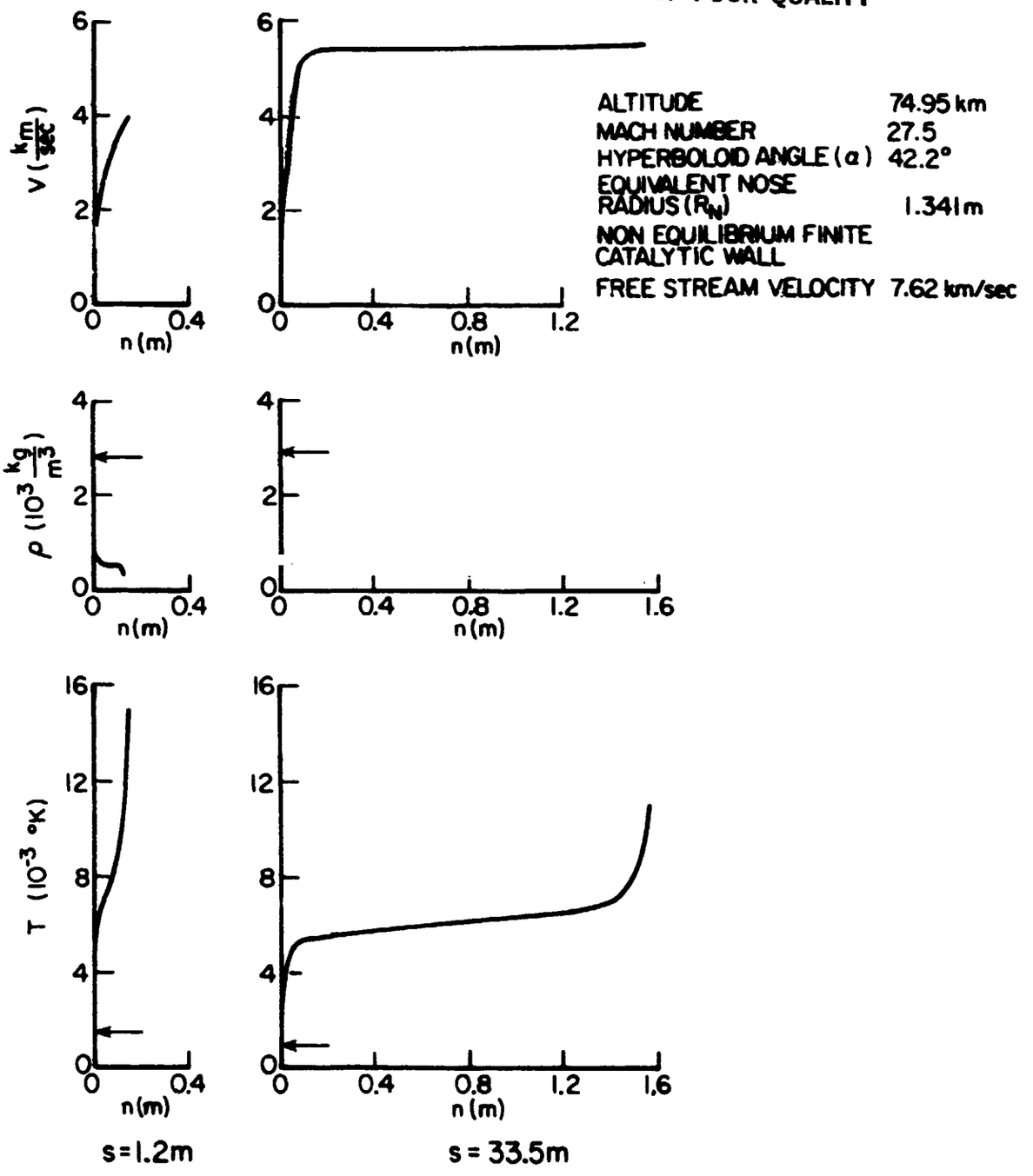

Figure 2. Velocity, temperature, and density outward from the windward centerline of a re-entering Space Shuttle orbiter at an altitude of 74.95 km. Conditions are shown for two locations s = 1.2 meters from the nose and 33.5 meters from the nose [Ref. 1].

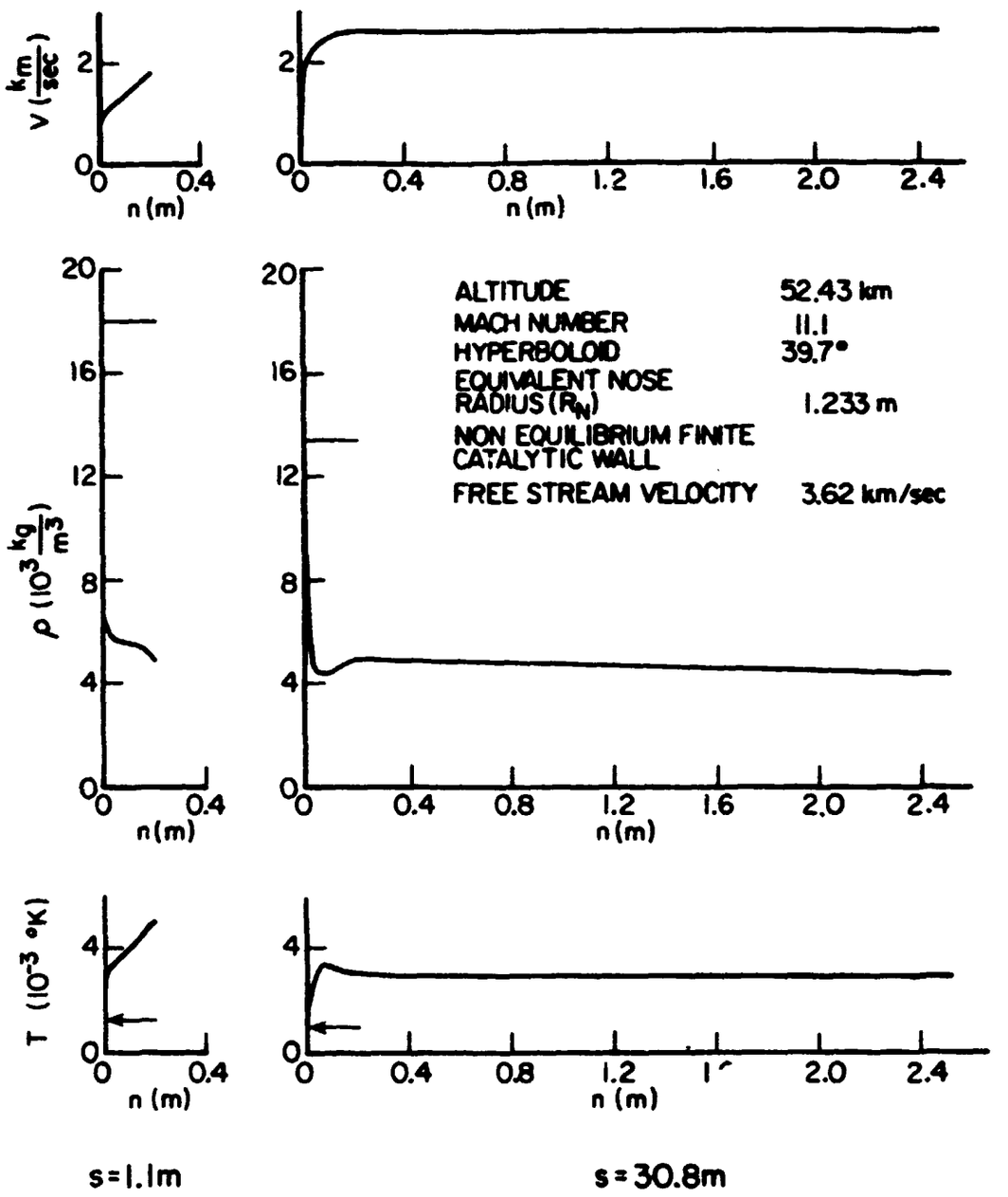

Figure 3. Velocity, temperature, and density outward from the windward centerline of a re-entering Space Shuttle orbiter at an altitude of 52.43 km. Conditions are shown for two locations s = 1.1 meters from the nose and 30.8 meters from the nose [Ref. 1].

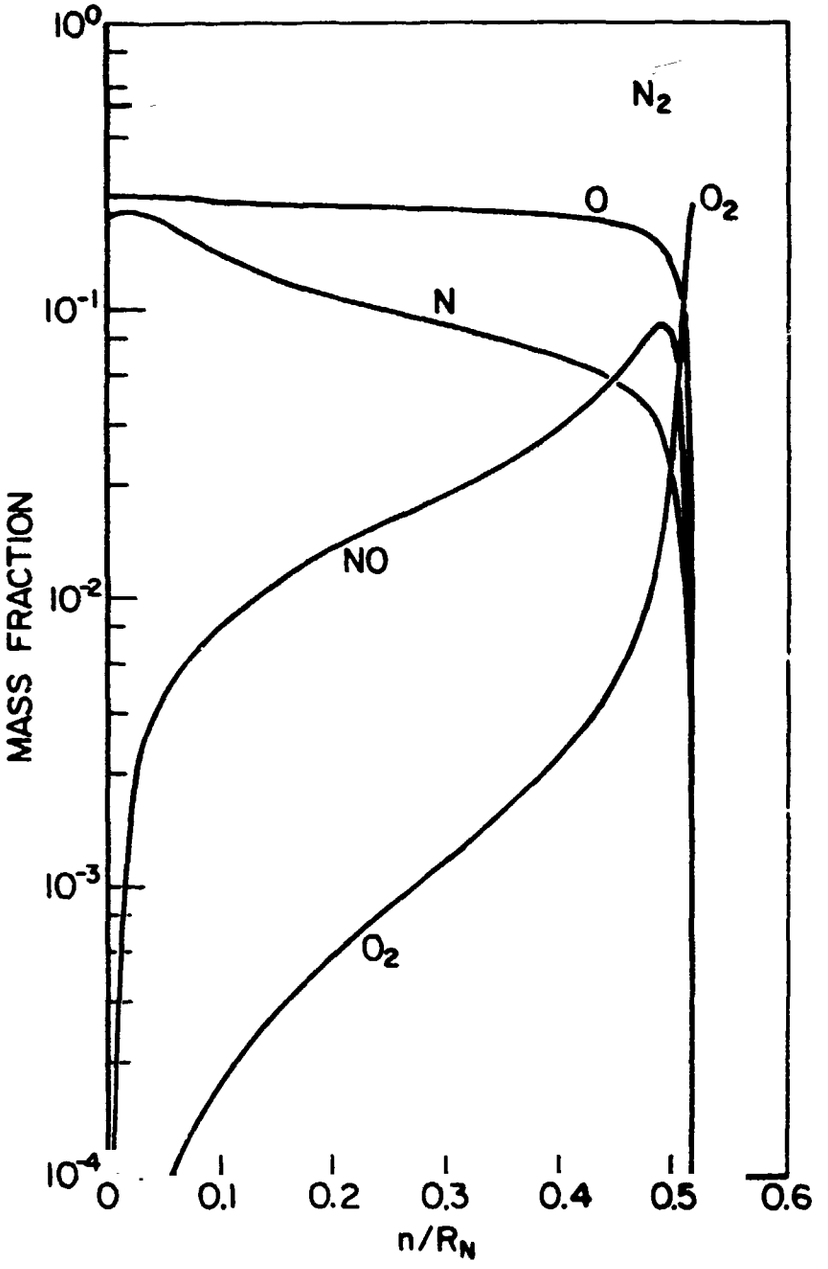

Figure 4. Species mass fraction for nonequilibrium flow with a non-catalytic wall [Ref. 1]. (42.2° Hyperboloid; $R_N = 1.34$ m; $s/R_N = 10.0$; Alt = 74.98 km; $M_\infty = 27.5$; $T_w = 1500°K$).

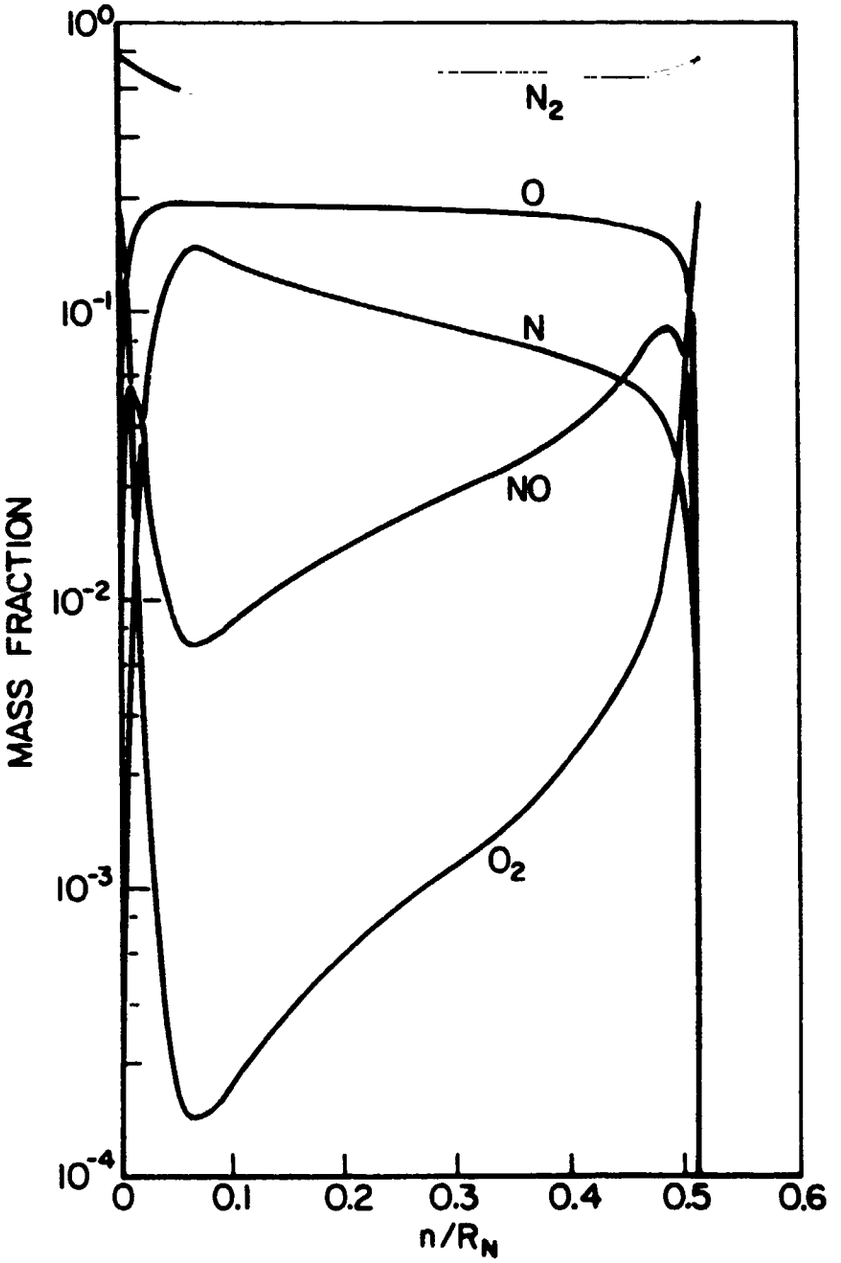

Figure 5. Species mass fraction for nonequilibrium flow with an equilibrium catalytic wall [Ref. 1]. (42.2° Hyperboloid; $R_N = 1.341$ m; $s/R_N = 10.0$; Alt = 74.98 km; $M_\infty = 27.5$; $T_w = 1500°K$).

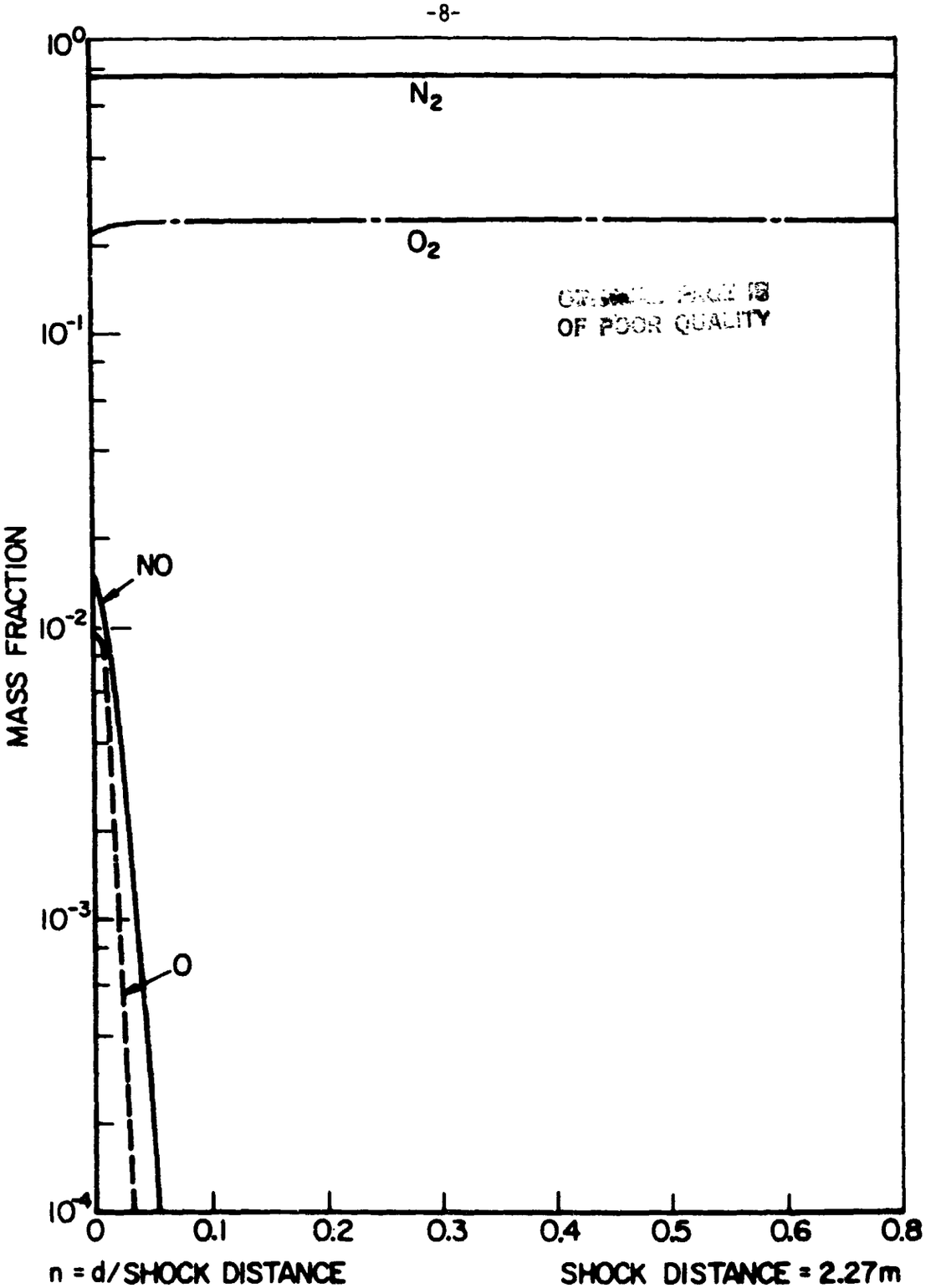

Figure 6. Species mass fraction for nonequilibrium flow with a finite catalytic wall [Ref. 3]. Alt = 47.67 km; M = 9.15; $\alpha = 34.8°$; $s/R_N = 25$.

Case	Altitude, km	u_∞, km/sec	ρ_∞, kg/m^3	M_∞	Equivalent Body* α ∿ deg	Equivalent Body* θ ∿ deg	Equivalent Body* R_N, m
1	74.98	7.62	3.80×10^{-5}	27.5	41.5	42.20	1.341
2	68.88	6.61	9.28×10^{-5}	22.6	40.2	40.85	1.286
3	64.92	5.94	1.55×10^{-4}	19.6	34.5	35.20	1.042
4	60.66	5.12	2.61×10^{-4}	16.4	31.8	32.40	.938
			STS-1 Conditions				
5	52.43	3.62	7.43×10^{-4}	11.1	39.0	39.7	1.233
6	48.16	2.98	1.33×10^{-3}	9.15	34.8	35.4	1.052
7	44.04	2.30	2.40×10^{-3}	7.14	30.9	31.6	.908

α angle of attack
* Hyperboloid with body half angle θ and nose radius R_N at zero degree angle of attack.

TABLE 1. Free-stream conditions and equivalent-body parameters.[2]

remains unverified until temperature profiles or species profiles can be measured. Density and velocity profiles as well as the location of the shock are also of significant interest. Near the nose, the shock stands less than 0.2 m from the surface, and substantial variations in velocity, temperature, density and species concentrations occur over small distances. These gradients are largest through the boundary layer where phenomena most directly related to the surface will occur.

The capabilities of the various non-intrusive detection methods are shown in Table 2. This table breaks the techniques into three categories. The first includes passive techniques which do not require illumination of the flow. Thermal emission naturally occurs from hot gases and particles and may be observed through a window and analyzed by an optical spectrometer. A mass spectrometer involves probeless samplings of multiple species in real time at the model surface and subsequent analysis to determine the gas species concentrations. The second category includes techniques which require active probing of the flow field with light or an electrom beam. The last category includes techniques which require both active probes and a foreign species seeded into the flow field. Note that, in theory, numerous ways are available for measuring both temperature and species concentrations.

The selection of the flow properties which would be the most valuable to measure was a topic of substantial discussion. Clearly, one would like to measure everything. Almost any measurement would give some check on the accuracy of the modelling. It was generally agreed however that species concentration or temperature would be especially useful as a check of the model. Certainly, a profile of one of these two variables would produce data of substantial interest. Also important are the density profile, shock

	TECHNIQUE	MEASUREMENT				
I.	Mass Spectrometry		Species Concentration			
	Thermal Emission	Temperature	Species Identity			
II.	Rayleigh Scattering	Temperature		Density	Velocity	
	Raman Scattering	Temperature	Species Concentration			
	Coherent Anti-Stokes Raman Scattering - CARS	Temperature	Species Concentration	Density		
	Mie Scattering					Particle Size/Density
	Laser Induced Fluorescence	Temperature	Species Concentration			
	Electron Beam Fluorescence	Temperature	Species Concentration			
III.	Laser Doppler Velocimetry				Velocity	Particle Size/Density
	Resonant Doppler Velocimetry	Temperature		Density	Velocity	

TABLE 2. Capabilities of Non-intrusive Detection Methods.

location, velocity profile, and the measurement of free-stream conditions. One of the most common concerns raised was the effect on the signal from the concentration of particles and the amount of thermal emission encountered in the flow. These two questions clearly affect the viability of several of the techniques and should be answered at an early stage. As will be evident in the following discussion, species measurements will be the most difficult to obtain with existing techniques. On the other hand, density profiles, temperature profiles, velocity profiles, particulate profiles, and the shock location may well be achievable by improvements in current technology.

A detailed discussion of each of the techniques and the methodology used for evaluation is presented in the appendices at the end of this report. Table 3 is a summary of the conclusions. This table is brokwn into five categories. The first category includes techniques which have undergone substantial laboratory testing and appear to have high promise. These are Rayleigh scattering, especially for density measurements and potentially for temperature and velocity measurements, and Mie scattering for particle concentrations, velocity, and size. The second category includes techniques which also appear promising but have either not been adequately demonstrated in the laboratory or their success depends strongly on the ability to identify and control the contribution to this signal by the noise. These are laser-induced fluorescence measurements of N, O, and NO concentrations and temperature (from NO) and mass spectrometry. Laser-induced fluorescence may produce profiles of the N, O, or NO concentrations which are sensitive indicators of the chemistry at high altitudes. Mass spectrometry may be capable of determining species concentrations within the boundary layer

CATEGORY	TECHNIQUE	PROJECTION
1	A. Rayleigh Scattering	Very Promising
	B. Mie Scattering	Very Promising
2	C. Laser-Induced Fluorescence	Promising
	D. Mass Spectrometry	Promising
3	E. Thermal Emission	Needs More Research
	F. Electron-Beam Fluorescence	Needs More Research
	G. Raman Scattering	Needs More Research
4	H. Coherent Anti-Stokes Raman Scattering - CARS	Little Promise
5	I. Laser Doppler Velocimetry	Requires Seeding
	J. Resonant Doppler Velocimetry	Requires Seeding

TABLE 3. Summary of Conclusions.

throughout the dissociated flow portions of the re-entry. The third category includes techniques which will require substantial additional work and are of questionable value. These are quantitative thermal emission, electron-beam fluorescence, and spontaneous Raman-scattering measurements of temperature and concentration. The fourth category includes techniques which appear to have very little promise. The only technique in this category is coherent anti-Stokes Raman scattering where the low densities, high temperature and crossed-beam phase-matching result in low signal strengths. A fifth category is reserved for those techniques which require seeding. It is currently impossible to determine the promise of these techniques; however it may be possible to use ablated material or naturally occurring particles in such a manner that the techniques may be vaiable. These are laser Doppler velocimetry and resonant Doppler velocimetry.

The most promising technique is Rayleigh scattering,which has been demonstrated to have the ability to measure density and temperature in the laboratory.[3] The scattering is observed at the same frequency as the laser, and therefore the signal is subject to substantial noise interference from scattering from particles which may be in the flow stream. Similarly, observations very close to the window may be difficult because of background light scattered from the window itself. Various species have different Rayleigh scattering cross sections. These do not vary substantially from that of N_2, and, since N_2 is always the major species, its cross section may be used for density and velocity measurements. For temperature measurements, however, the different molecular weights of the different species will cause different broadening of the scattered light, somewaht complicating the measurement. The Rayleigh technique involves a single laser

probe and could use an array of detectors so that a single laser pulse would yield an entire profile. It has been demonstrated in the laboratory that such a system may be integrated with a Mie scattering system for the detection of particles.[4] For example, when light is strongly scattered from a particle, simple logic in the detection system may be used to exclude that signal from the Rayleigh scattering measurement and separately register it in a particle counter. Thus, a single apparatus may conceivably yield pressure, temperature, velocity, and particulate profiles. Particle profiles will indicate which regions of the flow are most susceptible to interference and thus aid in the design of future experiments.

We also find laser-induced fluorescence from O, N, and NO to be a promising technique for both gas species concentration and temperature measurements. This application has not yet been fully demonstrated in the laboratory under conditions which can easily be related to the re-entry environment. Therefore, this technique has been included in the second catetory. These species are important as an indicator of the nonequilibrium chemical dynamics, particularly at high altitude. Although there are difficulties in using this technique to measure species concentrations, order of magnitude changes in species densities behind the shock should nonetheless be observable. The work of McKenzie et al. at NASA Ames has been largely directed towards the use of this technique for temperature measurements. Using the technique as he has done, it would appear that temperature profiles may be obtainable using two sequential laser pulses of different wavelengths. With this technique, scattering may be observed by multiple detectors as was true of Rayleigh scattering so that a profile may simultaneously be taken. Since a pulsed laser is used and fluorescence is observed over a rather narrow range of the spectrum, thermal emission can largely be excluded.

The evaluation of mass spectrometry was limited since no operational system for obtaining a gas sample through a flush orifice in the vehicle surface that is parallel to the flow has yet been developed. There are two major concerns associated with this technique. The first is that samples are taken from an area in such close proximity to the sampling port that they may not be indicative of the conditions away from the surface. The second is that the sample gas in passing through the orifice may under recombination or hit the wall and thus will not be truly indicative of the species concentrations in the boundary layer. Discussions with Dr. William McLean at Sandia and Drs. Daniel Seery and Med Colket of United Technologies indicate that a scavenging probe may be useful to alleviate this problem. For example, one could introduce hydrogen at the sampling port to interact with the oxygen atoms or O_{18} to interact with nitrogen atoms to produce a stable species that would, in effect, tag the original species. This method was originally suggested by Fristrom[5] and is currently being used for radical species diagnostics in combustion. A similar idea is being studied by George Wood at NASA Langley using isotopic labelling on the wall material. With proper care in the design of the inlet and a careful selection of pumping rates, this may be an effective way of obtaining species samples in close proximity to the surface.

Although thermal emission and electron-beam fluorescence may have the capability of yielding temperature and species concentrations, they are both better used for a qualitative than a quantative study of the flow field. For example, thermal emissions might enable one to determine the total column density which could then be used with laser-induced fluorescence to correct for pumping effects as has been suggested by Professor John Daily of the University of California. The thermally emitted light must be

collected over an integrated path, and, therefore, point measurements will be difficult if not impossible. Pressure and temperature effects may further confuse the analysis. Similarly electron-beam fluorescence has been developed as a flow-visualization tool and is not well adapted to quantitative measurements under these conditions. As Dr. William Hunter of NASA Langley noted, both quenching and temperature effects are not well understood. The electron beam has an advantage because it can operate at very high altitudes and might be useful as a qualitative probe for obtaining estimates of the low densities encountered in the early stages of re-entry.

Estimates for spontaneous Raman sensitivity based on the shot noise limit indicate that N_2 concentration measurements and N_2 vibrational temperature measurements should be possible over the entire range of altitudes. While O_2 and O concentration measurements are possible below 52 km and NO and N concentrations are not possible. This is encouraging but perhaps misleading, since even low level background noise from thermal emission or laser-induced particulate incandescence will render this technique useless. Further consideration of Raman scattering requires more information about the actual thermal emission and particle concentration conditions during flight.

Coherent anti-Stokes Raman scattering was found to be incapable of providing useful information under these conditions. The combination of low density and high temperature expected in flight, and the short interaction length (because of the required cross beam phase matching) produce a signal strength below the detection limit. Although multipoint measurements are possible, the required wide-angle crossed-beam matching to measure profiles would add to the experimental complexity.

If the flow field could be seeded either from the surface of the vehicle or by a cloud of seed material, then several other techniques become available. In particular, laser doppler velocimetry (LDV) may be an attractive way of measuring velocity profiles. Because of the very high velocities, however, conventional LDV systems are not appropriate. Several alternatives include simply monitoring the transit time scattering intensity profile as a particle passes through a single light beam as has been discussed by Dr. Don Holve of Sandia-Livermore, or the use of interferometers to observe the large spectral shifts of the light scattered by rapidly moving particles. Another possibility is to cross two collimated laser beams at a very slight angle to produce widely spaced interference fringes which reduces the modulation frequency of the particles passing through the laser beams. In this case, the depth of field becomes large, and a multiple detector system may be able to observe the velocity profile.

Similarly, if sodium atoms could be seeded into the flow, then the resonant Doppler velocimeter could be used to measure temperature, density, and velocity. This technique requires that the laser frequency be scanned and, thus, integration times of a few seconds would be expected. Here again, an array of detectors can simultaneously observe the entire flow-field profile. Using this technique, the velocity profiles should be easily discernible; however, quenching effects and the wide range of temperatures may lead to difficulty in the interpretation of temperature and density measurements.

3. Recommendations

Throughout this study many questions were raised concerning particle concentrations and the amount of thermal emission on the windward side of the re-entry vehicle as significant sources of noise in the signal.

These particles are also a potential source for seeding in laser Doppler velocimetry. In the case of Raman scattering, even relatively low levels of thermal emission or low densities of particles will prohibit its use. If the concentration of particles is sufficiently high, it will also obscure the Rayleigh scattering and laser-induced fluorescence signals and, if excessively high, eliminate laser Doppler velocimetry as an effective diagnostic tool. On the other hand, if the concentration of particles is low, Rayleigh scattering may be viable and might be used for temperature and velocity as well as density measurements. If the concentration of particles is too low, laser Doppler velocimetry may not be possible. Similarly, thermal emission, if excessive, may obscure the laser-induced fluorescence signal as well as Rayleigh scattering. For these reasons, we recommend that preliminary experiments be planned to measure the particle density and thermal emission in a flight environment. Such an experiment could combine with Mie and Rayleigh scattering using proper signal processing. With this information, preliminary estimates of the particle density and thermal emission intensity could be made and perhaps a density profile found.

The results indicate that Rayleigh and Mie scattering and laser-induced fluorescence are promising techniques but much development work is needed before a flight capplication can be considered. With regard to mass spectrometry, the technique has promise but is as yet unproven. A measurement of the concentrations would require the identification of dissociated or reactive species by techniques such as a reacting tag, either in the gas phase, or on the surface of the vehicle or inlet. The use of mass spectrometry in this manner is limited in the ability to probe beyond the surface.

References

1. Shinn, J.L., Moss, J.N. and Simmonds. A.L., 1982, "Viscous-Shock-Layer Laminar Heating Analysis for the Shuttle Windward-Symmetry Plane with Surface Finite Catalytic Recombination Rates," AIAA/ASME Joint Fluids, Plasmas, Thermophysics and Heat Transfer Conference, June 7-11, 1982, St. Louis, Missouri,

2. Scott, D.C., 1981, "Space Shuttle Laminar Heating with Finite Rate Catalytic Recombination," AIAA Paper 81-1144, 1981.

3. Dibble, R.W. and Hollenbach, R.E., 1981, "Laser Rayleigh Thermometry in Turbulent Flames," Eighteenth Symposium (International) on Combustion, Waterloo, Canada, 1981.

4. Schefer, R.W., Dibble, R.W. and Driscoll, J.F., 1982, "Mass Fluxes $\overline{\rho' u'}$ and $\overline{\rho' v'}$ Measured in a Turbulent Nonpremixed Flame," Spring Meeting of the Western States Section of the Combustion Institute, Paper #NSSCI-82-35, 1982.

5. Fristrom, R.M. and McLean, W.J., 1982, "The Determination of Atom and Radical Concentration in Flames Using a Scavenger Microprobe," Presented at the Canadian Section of the Combustion Institute, Spring Meeting, May 1982.

Acknowledgments

The authors gratefully acknowledge the extensive advice and comments of a large number of researchers. Most of these scientists are current engaged in related work and all provided valuable perspective for this study.

Princeton University:

G. Bienkowski	I. Kennedy	A. Smits
S. M. Bogdonoff	M. Littman	
D. Dolling	G. Settles	

NASA/Ames:

R. McKenzie

NASA/Langley:

D. Eide	J. Jones	J. Shinn
J. Hoppe	B. Lewis	K. Sutton
W. Hunter	J. Moss	G. Wood

United Technologies, Hartford, Connecticut:

M. Colket	M. Sabielski
A. Eckbreth	D. Seery

University of California, Berkeley, California:

J. Daily
L. Talbot

Sandia National Laboratory, Livermore, California:

R. Cattolica
R. Dibble
M. Dyer
W. Flower
D. Holve
W. McLean
L. Rahn
G. Ramback
R. Schefer
J. R. Smith
P. Witze

Stanford University, Stanford, California:

D. Baganoff
D. Bershader
R. Hansen
C. Kruger

APPENDIX A. RAYLEIGH SCATTERING

h	6.6256×10^{-34} joule-sec	Planck's constant
L	meters	sample volume length
n_p		number of pulses per measurement interval
N_i	$meters^{-3}$	number density of species i
$P_{RAYLEIGH}$	watts	Rayleigh scattered signal power
P_o	watts	incident laser power
Q_i	$meters^2$/ steradian-molecule	Rayleigh cross section of species i
$S/N_{RAYLEIGH}$		Rayleigh scattering signal to noise ratio
Δt	second	laser pulse duration
η_c		efficiency of the collection optics
η_D		efficiency of the detector
λ	meters	laser wavelength
ν	Hertz	Rayleigh radiation frequency
Ω_c	steradians	solid angle of collection optics

TABLE A.1 List of Symbols.

Rayleigh scattering is an elastic scattering process with an intensity proportional to the density of scattering molecules. It is several orders of magnitude stronger than Raman scattering and weaker than fluorescence processes but lacks the gas species selectivity of Raman scattering. Since the scattered light is at the same frequency as the source, Rayleigh signals are easily obstructed by Mie scattering (in particle laden environments) or

laser light reflected from optic surfaces. In addition to density measurements, Rayleigh scattering has been used for temperature measurements in constant pressure, non-reactive flows where the density and temperature are related through the equation of state.[A.1] The Doppler shift $(\lambda - \lambda')$ and broadening $\Delta\lambda$ of the Rayleigh line can also be used to measure the velocity and temperature, respectively.[A.2] The effects of velocity and temperature on the Rayleigh line are shown schematically in Figure A.1. The Rayleigh scattering cross-section is species dependent, therefore a change in Rayleigh signal strength or line shape can result if composition changes as well as density or temperature changes occur.

The Rayleigh scattered power is given by the following expression:

$$P_{RAYLEIGH} = P_o \, L \, \Omega_C \, \eta_C \, \eta_D \sum_i N_i \, Q_i \qquad (A.1)$$

where P_o is the power of the incident laser beam, L is the length of the incident laser beam of the sample volume from which scattered light is collected, Ω_C is the solid angle of the collection optics, η_C is the efficiency of the collection optics, η_D is the detector quantum efficiency, N_i is the number density of species i and Q_i is the Rayleigh cross section for species i. A typical Rayleigh scattering experimental configuration is shown in Figure A.2. Light is usually collected at 90° to the source laser, however collection at other angles is common.

The sensitivity and accuracy of Rayleigh scattering for total density measurements was evaluated in terms of the minimum detectable density for a given signal to noise ratio. The noise was assumed to be shot noise which is equal to the square root of the number of detected Rayleigh photons. This leads to a signal to noise ratio:

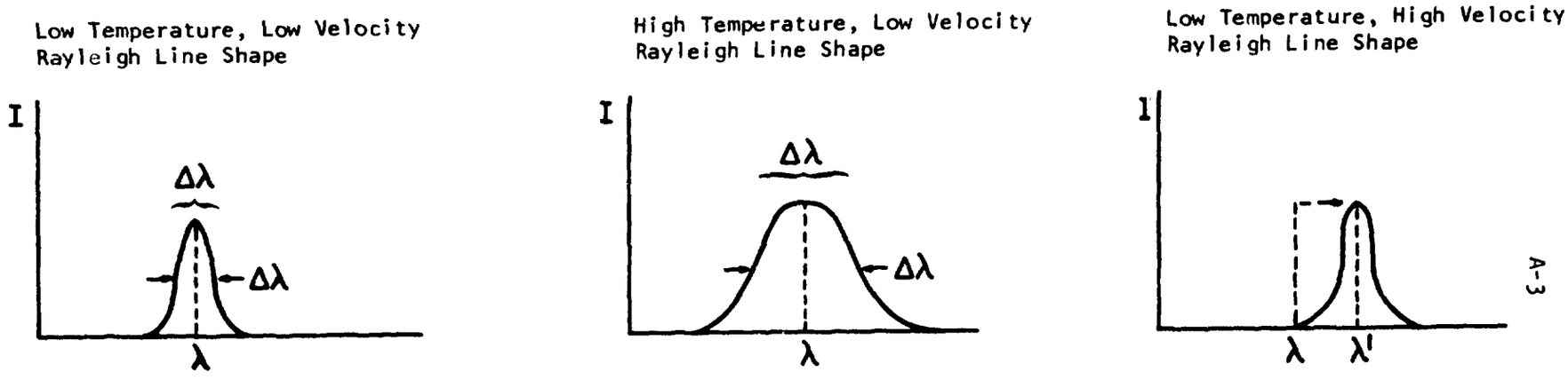

Figure A.1 The effect of temperature and velocity on Rayleigh spectrum.

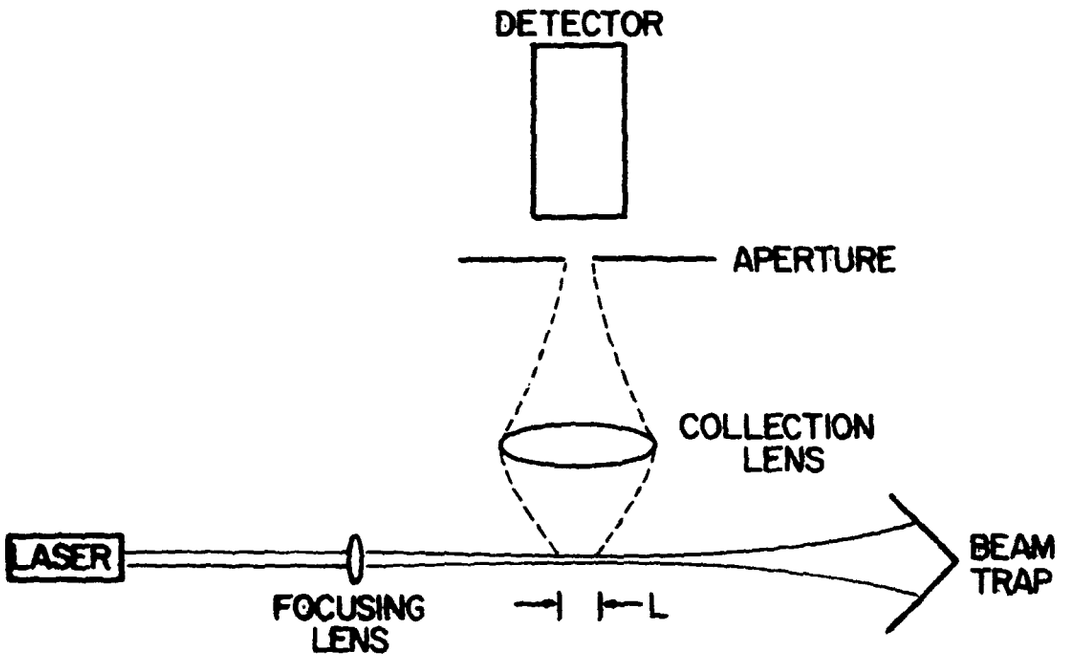

Figure A.2 Typical Rayleigh Scattering Experiment.

$$(S/N)_{RAYLEIGH} = (P_{RAYLEIGH}\ \Delta t\ n_p/h\nu)^{1/2} \qquad (A.2)$$

where Δt is the pulse duration, n_p is the number of pulses during the measurement interval, h is Planck's constant and ν is the radiation frequency.

The experimental parameters used in equations (A.1) and (A.2) to determine the minimum detectable total density are those given in Table A.2. Two lasers were considered, a krypton fluoride (KrF) excimer laser and a copper vapor laser. The KrF laser has a higher average power. Its UV output also leads to larger cross-sections and greater detector quantum efficiencies. The copper vapor laser produces a narrower output linewidth and has higher efficiency. Based on the rate of descent of the Shuttle, an integration time of 10 seconds was chosen. The Rayleigh cross section for N_2 was used in this estimate, i.e. 8×10^{-28} cm^2/str-molecule at 514.5 nm. For a signal to noise ratio of 10, the resultant minimum detectable number density is 1.2×10^{12}/cc with the KrF laser and 1.1×10^{12}/cc with the copper vapor laser. Both of these values are less than the minimum density at the highest altitude. This result agrees well with a detection limit estimate made by Robert Dibble of Sandia-Livermore Laboratory who extrapolated from detection limits he routinely observes in the laboratory. He also estimated the error due to variations in composition to be less than $\pm$15%. Therefore when we assume the shot noise limit, the use of Rayleigh scattering for total density measurements over the entire range of altitudes appears very promising. The problem of Mie scattering from particles is an important concern, since it could be orders of magnitude greater than the Rayleigh scattering; however, if the particle concentration is not too high it is possible to identify and reject the larger signals due to particles.[A.3]

		KrF Laser*	Copper Vapor Laser**
Incident Laser Power in Sample Volume	P_o	6.25 MW	0.1 MW
Pulse Length	Δt	16 nsec	50 nsec
Repetition Rate		25/sec	5×10^3/sec
Wavelength	λ	249 nm	510 nm
Detector Quantum Efficiency	η_D	0.35	0.1
Collector Optics Efficiency	η_C	0.1	0.1
Optics Collection Angle	Ω_C	0.01 str	0.01 str
Scattering Length	L	5 mm	5 mm

* Lambda Physik Model EMG 201.
** Plasma Kinetics Model 751.

TABLE A.2 Values Used for Rayleigh Scattering Signal to Noise Estimates.

To use Rayleigh scattering for temperature and velocity measurements, a narrow line width laser (which rules out the use of the KrF laser) and a scanning Fabry-Perot etalon with adequate resolution must be used in order to resolve the Doppler shift and broadened line width which will both be of the order of 0.1 cm^{-1}. The number of detected photons will in turn be reduced, which will increase the minimum detectable number density to approximately 10^{15}/cc. Since the minimum nitrogen density at 75 km altitude is also 10^{15}/cc,[A.4] the Rayleigh temperature and velocity measurements will be possible at all altitudes below 75 km throughout the flow field. For the temperature measurement it will be necessary to correct for composition changes, perhaps using the calculated Rayleigh lineshape,[A.2] although the densities of species other than nitrogen are so low that this latter effect is likely to be negligible.

References

A.1 Dyer, M.T., 1979, "Rayleigh Scattering Measurements of Time-Resolved Concentration in a Turbulent Propane Jet," AIAA Journal 17, No. 8.

A.2 Cattolica, R., Robben, F. and Talbot, L., 1976, "The interpretation of the Spectral Structure of Rayleigh Scattered Light from Combustion Gases," AIAA Paper No. 76-31.

A.3 Schefer, R.W., Dibble, R.W. and Driscoll, S.F., 1982, "Mass fluxes $\rho'u'$ and $\rho'v'$ Measured in a Turbulent Nonpremixed Flame," Presented at 1982 Spring Meeting of the Western States Section of the Combustion Institute, Paper WSS/CI 92-35.

A.4 Shinn, J.L., Moss, J.N. and Simmonds, A.L., 1982, "Viscous-Shock-Layer Laminar Heating Analysis for the Shuttle Windward-Symmetry Plane with Surface Finite Catalytic Recombination Rates," AIAA/ASME Joint Fluids, Plasmas, Thermophysics and Heat Transfer Conference, June 7-11, 1982, St. Louis, Missouri.

APPENDIX B. MIE SCATTERING

The presence of particles which have ablated from the Space Shuttle orbiter tiles during entry are of interest for several reasons. Most notably, they represent a potential noise source for all of the optical diagnostics. Mie scattering, together with laser-induced incandescence from particles and thermal emission could interfere with other optical measurements, depending on the particle density and size distribution. It is essential to obtain information about the severity of these potential problems before implementing any of the optical techniques.

If particles are present, they may be usable as a diagnostic seed for measuring velocity and temperature. Shortly after the particles are ablated from the vehicle surface they will be accelerated to the gas velocity. The time required to reach the gas velocity will depend on the particle mass. The depth of penetration into the boundary layer will depend on the perpendicular momentum with which the particle was released from the surface. One can expect that within a certain distance from the surface there will be some particles which have not yet equilibrated with the gas velocity. To use these particles as a gas diagnostic seed it is necessary to determine which particle velocities correspond to the gas velocity. One way of doing this is to take the velocity of the fastest particles to be that of the gas. Another method is to measure both the size and the velocity simultaneously and to assume that the small particles are most likely to be travelling at the gas velocity. Such information could be obtained from a dual-beam laser Doppler velocimetry system where the particle size is obtained from the visibility parameter of the Doppler burst. Unfortunately, this method requires a priori knowledge of the particle size range, since the

visibility parameter is single valued over only a limited range of particle sizes. No other simultaneous velocity and particle sizing technique has been demonstrated to a reasonable degree of satisfaction. Dr. Donald Holve of Sandia-Livermore suggested using single-beam methods, i.e. transit time velocimetry for velocity and pulse height detection for particle size, whereby velocity and size distributions could be obtained but no velocity-size correlations.[B.1,B.2] Techniques using the angular distribution of the Mie scattered light to obtain particle size would be difficult to interpret because of the unknown and irregular particle shapes. Additional details on velocity measurement techniques can be found in the sections on laser Doppler velocimetry and resonant Doppler velocimetry.

Any particles present in the flow could also be used to give an indication of the gas temperature by looking at the spectral distribution of their thermal emission; however, some assumptions about the particle emissivity would be required. The question of thermal equilibrium between the particle and the gas would also have to be considered.

Obtaining particle data requires a small window in the windward side of the re-entry vehicle. This window would provide optical access to the flow within the boundary layer to obtain data relative to the thermal emission intensity and spatial characteristics of the surrounding gas and particles. Mie scattering from a laser beam projected out through the window would provide an estimate of the particle number density and, possibly, the size and spatial distribution.

A combined Mie scattering and Rayleigh scattering experiment may be conducted through the window and might best provide a method for determining particle densities. For such an experiment, particles with diameters less than approximately 0.1 μ will not be easily distinguishable from the

background gas. Larger particles can be seen due to their strong light scattering. A high repetition pulsed laser focused into the flow would provide strong scattering from the particles and weak scattering from the gases. The short pulse length of the laser freezes the flow, so the pulse either scatters from a particle in the observation zone, or it does not. In this manner, particle densities may be counted by knowing the size of the interaction zone. Simultaneously, gas densities may be found from the strength of the scattering from the gas in the absence of a particle. Operation of the detector in between laser pulses could also provide thermal emission data. Such an experiment would generate essentially all the information needed to establish the viability of the various flow diagnostic techniques and could simultaneously yield gas density information.

References

B.1 Holve, D.J., 1980, "In Situ Optical Particle Sizing Technique," J. Energy 4, No. 4, pp. 176-183.

B.2 Holve, D.J., 1982, "Transect Timing Velocimetry (TTV) for Two-Phase Reacting Flows," Combustion and Flame 48, No. 1.

APPENDIX C. LASER-INDUCED FLUORESCENCE

Laser-induced fluorescence has the potential of measuring rotational and vibrational temperature and species concentration and of performing density sensitive flow visualization. Generally, one or more laser beams are directed into the flow to excite a particular species to a higher energy level. A detector then collects the fluorescence as the gas relaxes back to its initial state after a characteristic lifetime. The detector may be configured to monitor any position along the laser beam to give good spatial resolution (up to $\sim 10^{-2}$ mm).[C.1] The fluorescence intensity is proportional to the population of absorbing molecules in the radiating upper energy level during the excitation process. The population of these levels is related to the total number density of molecules through the rate equations which include the processes of spontaneous emission, stimulated emission, absorption, collision quenching, rotational redistribution, and vibrational redistribution. Unfortunately, the parameters describing these competing processes such as the identities, concentrations, and quenching rates of all possible collision partners are not completely understood.

Temperature and species-concentration measurements using laser-induced fluorescence have been demonstrated at pressures equal to or less than one atmosphere and at temperatures up to those found in typical combustion environments (about 2000°K).[C.1] The most frequently treated species has been OH because of its important role in combustion kinetics; however, work has also been performed on numerous other systems including NO, N, and O[C.2-C.5] which are of interest in this study.

Several schemes have been proposed to account for the effect of collisional quenching of radiation on the experimental results. One method, as

first proposed by Piepmeier,[C.6] requires saturating at the upper energy level and thereby eliminating the dependence on laser intensity as well as the need to correct for quenching. Since complete saturation is difficult to achieve, Baronovski and McDonald[C.7] proposed and demonstrated a partial saturation technique whereby one can extrapolate to the complete saturation limit. Another method, proposed and demonstrated by Stepowski and Cottereau,[C.8] does not require saturation but requires that the laser pulse duration be shorter than the time for steady state conditions to be reached. The quenching rate then can be related to the fluorescence decay curve. The required laser-pulse duration and the fluorescence decay rate will depend on the gas pressure and temperature. Other methods include the use of empirical quenching corrections as in the work of Muller et al.[C.9] and the use of detailed multi-level models as in the work of Chan and Daily[C.10] and that of Kotlar, Gelb and Crosley.[C.11]

The most promising approach at low density conditions is to determine the quenching rate from the fluorescence decay rate as has been done by Stepowski and Cottereau[C.8] for OH in a low pressure flame, and by Bischel, Perry, and Crosley[C.2] for both O and N atoms in a low pressure flow discharge. Based on the results of the latter work and the similarity between the excited electronic state lifetimes for OH and NO, a laser pulse width of less than 5 nsec is required. For O and N atom fluorescence, two-photon absorption is required because the first resonance transition lies far into the VUV. As Bischel et al.[C.2] have demonstrated, one would detect the resultant near IR fluorescence. For NO, the resonance transition can be accessed by either single or two-photon absorption. The disadvantage of the two photon process is that it is non-linear in laser power. The advantage is that it is less difficult to generate tunable, stable, high-power visible

radiation than the UV radiation required for the single photon process. There was no concensus among the researchers interviewed on this point. In either case, the best laser system would be a Nd:YAG pumped dye laser using frequency doubling and/or Raman shifting to generate the required UV wavelengths.

After accounting for quenching, the fluorescence intensity gives the population of the lower energy level before laser excitation which can then be related to the total population if the temperature is known. The fluorescence technique can also be used to find the temperature by measuring the population of two or more energy levels, since the ratio of the population of any two levels is equal to the ratio of the corresponding Boltzmann factors.

Of parti[illegible]terest to this study is the work of McKenzie and Gross[C.3] who have demonstrated single laser pulse temperature measurements of NO seeded into a flow o. nitrogen. Excitation by two photons of a selected rotational level from two distinct initial rotational levels is performed in rapid succession and the fluorescence monitored. The ensuing fluorescence intensity in each pulse can be related to the rotational populations in the two initial ground states and the ratio related to the rotational temperature. Since only the ratio of energies absorbed needs to be known, the redistribution of energy among rotational and vibrational levels of the excited state and their non-radiative quenching have a negligible effect on the measurement. The quenching is negligible providing it does not significantly vary from one rotational level to the next and broad-band detection is used. McKenzie considered the transition $A^2\Sigma^+$, $v' = 0 \rightarrow X^2\Pi_{1/2}$, $v'' = 0$ in NO from the $J'' = 7\frac{1}{2}$ rotational level, since it has the largest absorption coefficient at room temperature and is separated far enough from other lines

to allow selective excitation. He obtained a signal-to-noise ratio (S/N) in the quantum noise limit of 200 for a single 1 millijoule pulse energy of 5 nsec duration. The NO concentration which he used was 2×10^{14} cm^{-3} at room temperature, and the size of the probe volume was 0.1 mm x 1.0 mm. As may be seen from Figure 5 in the main section of this report the maximum density of NO in the flow surrounding the re-entry vehicle is an order of magnitude higher at an altitude of 75 km. The temperature is also higher; so the NO molecules distribute over more states, thus lowering the density in any given vibrational rotational level. The signal is further reduced by increased quenching because of the higher temperature.

The minimum NO density downstream of the shock is 10^{14} cm^{-3} and the NO may have a translational temperature as high as 16,000°K. Scaling calculations were made for both 16,000°K and 3000°K and yielded a S/N of 9 and 40, respectively, for a single 1 mJ pulse. The lower temperature was chosen because of the expectation that internal modes and chemical reactions will rapidly cool the translational energy of the gas, substantially lowering the rotational temperature. Increasing the laser's intensity to improve the S/N is limited by Stark broadening. The broadening reduces the laser energy coupling into the transition and may cause several lines to coalesce so that a particular rotational level may no longer be preferentially pumped. McKenzie has not yet quantified this limitation.

To determine the density detectability limit for a quantum noise limited signal to noise ratio of 10, a laser operating at 10 pulses per second with 1 mJ per pulse was considered. The integration time was assumed to be 10 seconds. The NO detectability then was found to correspond to 1.5×10^{13} cm^{-3} and 7.5×10^{11} cm^{-3}, at temperatures of 16×10^{3}°K and 3000°K, respectively. The NO number density in most of the region between the shock and the vehicle

surface at an altitude of 75 km is predicted to be between 10^{14} cm^{-3} to 10^{15} cm^{-3}. A comparison of Figures 4 and 5 in the main text of this report shows that the NO concentration behind the shock decreases significantly as the altitude decreases and by 47 km it is negligible except close to a catalytic wall. Consequently, the laser-induced fluorescence technique is only useful at the higher altitudes.

In summary, measurements of NO, N, and O concentrations and NO rotational temperature appear feasible at 75 km where measurable concentrations could be expected. Such measurements have been demonstrated under similar but not identical conditions. Solutions to the problems of thermal emission from the high temperature gas and hot particles behind the shock and Mie scattering from particles should be investigated before obtaining a laser-induced fluorescence measurement.

References

C.1 Cattolica, R., 1981, "OH Rotational Temperature from Two Line Laser Excited Fluorescence," Applied Optics 20, pp. 1156-1166.

C.2 Bischel, W.K., Perry, B.E. and Crosley, D.R., 1982, "Detection of Fluorescence from O and N Atoms Induced by Two-Photon Absorption," Applied Optics 21, pp. 1419-1429.

C.3 McKenzie, R.L. and Gross, K.P., 1981, "Two-Photon Excitation of Nitric Oxide Fluorescence as a Temperature Indicator in Unsteady Gasdynamic Processes," Applied Optics 20, pp. 2153-2165.

C.4 Bradshaw, J. and Davis, D.D., 1982, "Sequential Two-Photon-Laser-Induced Fluorescence: A New Method for Detecting Atmospheric Trace Levels of NO," Optics Letters 7, pp. 224-226.

C.5 Bradshaw, J., Rodgers, M.O. and Davis, D.D., 1982, "Single Photon Laser-Induced Fluorescence Detection of NO and SO_2 for Atmospheric Conditions of Composition and Pressure," Applied Optics 21, pp. 2493-2500.

C.6 Peipmeier, E.H., 1972, "Theory of Laser Saturated Atomic Resonance Fluorescence," Spectr. Acta. 27B, pp. 431-443.

C.7 Baronovski, A.P. and McDonald, J.R., 1977, "Measurement of C_2 Concentrations in an Oxygen-Acetylene Flame: An Application of Saturation Spectroscopy," J. Chem. Phys. 66, pp. 3300-3301.
Baronovski, A.P. and McDonald, J.R., 1977, "Application of Saturation Spectroscopy to the Measurement of C_2, $3\pi_u$ Concentrations in Oxy-Acetylene Flames," Applied Optics 16, pp. 1897-1901.

C.8 Stepowski, D. and Cottereau, M.J., 1979, "Direct Measurement of OH Local Concentration in a Flame from the Fluorescence Induced by a Single Laser Pulse," Applied Optics 18, pp. 354-356.

C.9 Muller, C.H., Schofield, K., Steinberg, J. and Brorda, H.P., 1978, "Sulfur Chemistry in Flames," Seventeenth International Symposium on Combustion, p. 867.

C.10 Chan, C. and Daily, J.W., 1979, "Measurement of OH Quenching Cross-Sections in Flames Using Laser Induced Fluorescence Spectroscopy," Presented at the Western States Section of the Combustion Institute, Spring Meeting, Provo, Utah, Paper #79-20.

C.11 Kotlar, A.J., Gelb, A. and Crosley, D.R., 1980, "A Multilevel Model of Response to Laser Fluorescence Excitation in OH," Laser Probes for Combustion Chemistry, Editor Crosley, D.R., ACS Symposium Series 134, American Chemical Society, Washington, D.C.

APPENDIX D. MASS SPECTROMETRY

Mass spectrometry can be used to measure the concentrations of O_2, N_2, NO, O, and N over the entire range of densities that are expected during reentry. A mass spectrometer with a fixed collector plate detector which would enable simultaneous measurements of all these species in real time has been proposed by George Wood of NASA Langley. A similar spectrometer has been built and successfully tested for NASA by Lehotsky.[D.1] Dr. Martin Zabielski of United Technologies pointed out that the sample flow rate between the altitude of 80 and 40 km would change by approximately a factor of 10 for a fixed orifice area and given pumping system. He suggested that the pumping system be designed for 40 km and then simply overpumped at higher altitudes. This would permit continuous measurements to be made at all altitudes.

If effusive collection is used (the collection orifice diameter less than the mean free path), the sample would come from within a few mean free paths of the surface. This may cause difficulty, since the gas composition within a few mean free paths of the collection orifice may be affected by the presence of the orifice if the orifice and Space Shuttle orbiter wall material have different catalytic properties. Dr. Daniel Seery of United Technologies suggested that it may be possible to use a larger orifice and collect the sample by modest pumping which, because of the low densities, would cause minimal disturbance to the flow field. By pumping on the orifice, one would extend the sample volume further out into the flow field, beyond the region which is affected by the local surface reactions.

A major problem in using mass spectrometry is the extraction of a sample which reflects the true composition of these gases. Radical species, particularly O and N atoms, quickly react or recombine. Because of the

thickness of the tiles protecting the surface of the re-entry vehicle and the necessity to thermally insulate the mass spectrometer from the exterior temperatures, the sample must travel several inches before being analyzed. In order to minimize the effect on the local flow field, the passageway through the tiles should be short. If the sample travels through a long narrow passageway, both walls and gas phase collisions, and in turn O and N atom recombination reactions, are probable. Wood has proposed selecting the wall material such that the O and N atoms selectively react upon collision with the wall, producing a stable and identifiable species which would in effect serve to tag the original atomic species. Drs. Daniel Seery and Med Colket of United Technologies and Dr. Robert McLean of Sandia-Livermore all suggested using the scavenging probe concept proposed by Fristrom and recently demonstrated by Fristrom and McLean.[D.2] Here, the sample is immediately diluted at the orifice with a gas stream containing a species which selectively reacts with either the O or N atoms to produce a stable and identifiable species. This species then serves to tag the original atomic species. If this stable product were already present in the sample then it might be possible to distinguish between the sample and the tag molecule by using different isotopes. Possible interference with the natural flow and chemistry within the boundary layer should be examined before using this probe concept.

Another possibility suggested by Seery and Colket is to extend a traversing scavenging probe out into the boundary layer in order to extract samples at different distances from the wall. They felt that because of the very high velocities that all appreciable disturbances to the flow field would be convected downstream and would not affect the measurement. They did point out, however, that when the flow is supersonic, as it is outside

the subsonic boundary layer, there will be a shock in front of the probe which may substantially alter the sample's composition and the aerodynamic and aerothermodynamic performance.

Using a scavenging probe to extract the sample with subsequent mass spectroscopic analysis is a promising technique for determining the concentrations of N_2, O_2, O, and N near the wall. This probe could be used to obtain samples of the species at points away from the wall by using a traversing probe or by modest pumping rates, providing the natural flow and chemistry is not disturbed.

References

D.1 Lehotsky, R.B., 1973, "A Mass Spectrometer Sensor System for Metabolic Analysis and Atmospheric Monitoring on Skylab and Future Manned Spacecraft," Proceedings of the 21st Annual Conference of Mass Spectrometry and Allied Topics, May 20-25, 1973, San Francisco, CA, p. 403.

D.2 Fristrom, R.M. and McLean, W.J., 1982, "The Determination of Atom and Radical Concentration in Flames Using a Scavenger Microprobe," Presented at the Canadian Section of the Combustion Institute, Spring Meeting, May 1982.

APPENDIX E. THERMAL EMISSION

Symbol	Units	Description
A_{jk}	sec^{-1}	Einstein spontaneous emission coefficient for level j to k
C_i		concentration of species i
c	meters/sec	speed of light in vacuum
d	meters	thickness of radiating layer
E_j	joules	energy of the j^{th} energy level
F		f number of collection optics (lens focal length/lens diameter)
g_j		degeneracy of the j^{th} energy level
h	6.6256×10^{-34} joule-sec	Planck's constant
I_{jk}	watts/$meter^2$	emission intensity from level j to level k
I_o	watts/$meter^2$	blackbody radiation intensity per unit wavelength
I_λ	watts/$meter^2$	emission intensity per unit wavelength
J_λ		emission coefficient per unit wavelength
K_λ		absorption coefficient per unit wavelength
K'_λ		absorption coefficient per unit wavelength
k	1.38054×10^{-23} joules/°K	Boltzmann's constant
m	Kg	mass
s'	meters	displacement along a ray of light
T	°K	temperature
λ	meters	wavelength
$\Delta\lambda$	meters	width of spectral filter in wavelength
λ_{jk}	meters	emission wavelength for transition from level j to level k

Symbol	Units	Description
$\Delta\nu$	Hertz	line width--full width at half maximum
ρ	kg/meters^3	density
τ		optical length

TABLE E.1 List of Symbols.

Highly excited atoms and molecules, as well as high temperature particles, will emit light in the visible range of the spectrum. For the most part this light will constitute a noise source for other optical non-intrusive techniques. It may, however, be used to give a rough measurement of temperatureature, species identity, and provide light for flow visualization. By tracking the motion and the spectral emission of hot particles their temperature and velocity might also be determined. Thermal emission will occur from all hot regions in the flow and the collected signal is essentially the light projected from each of these regions onto the surface aperture. Consequently, the signal is integrated over a pathlength, so this technique cannot be used to yield good spatial resolution. Practically, the highest temperature portion of the flow occurs just behind the shock at high altitudes so the region responsible for the thermal emission may be reasonably well delineated. The interpretation of flow parameters such as species and temperature depends largely on the optical thickness of the emitting gases. Over the temperature and flow regions of interest, the gases are optically thin. A major source of uncertainty in signal interpretation in the optically thin region is from incomplete knowledge of quenching rates and Franck-Condon factors.[E.1]

In a nonequilibrium gas, the different energy modes of the atoms and molecules will not be in thermal equilibrium. Often each mode may be

characterized by a different "temperature." Usually the translational modes quickly equilibrate with the surrounding medium and thus most accurately reflect what is conventionally known as the temperature. The translational temperature of an optically thin gas can be measured by resolving the spectral line profile of the emission from a particular transition. The profile has to be observed with an interferometer to achieve sufficient resolution. For a purely thermally broadened spectral line, the full frequency width at half maximum intensity, $\Delta\nu$, is related to the gas temperature, T, by,[E.2]

$$T = \left(\frac{\Delta\nu\ \lambda_{21}}{2}\right)^2 \frac{m}{2k\ \ln 2} \qquad (E.1)$$

where λ_{21} is the emission wavelength, m is the mass of the species, and k is Boltzmann's constant. If the temperature is to be measured in this manner one must first do a deconvolution to remove the broadening effect due to collisions and the less than perfect resolution of the interferometer.

If the equivalent "temperature" is desired for the internal modes of the atom or molecule, the ratio of the emission intensities for various spectral lines must be measured. For each spectral line the emission intensity, I_{21}, from an optically thin source is

$$I_{21} = K\ g_2 \frac{A_{21}}{\lambda_{21}} \exp(-E_2/kT) \qquad (E.2)$$

where K is a constant, g_2 is the degeneracy of the excited level, A_{21} is the Einstein spontaneous emission coefficient of the transition, E_2 is the energy of the excited state, and T is the effective temperature. This fluorescence is substantially reduced by the presence of quenching which itself is temperature dependent. In an effort to remove the effects of quenching, emission from two similar excited states may be observed so that one may approximate the quenching factor of each to be identical. This is similar

to the method used for laser induced fluorescence measurements discussed in Appendix C.

Both the measurement of translational temperature and the measurement of the effective temperature of internal modes depend on the gas being optically thin. As the gas turns optically thicker, the emission spectrum approaches that of a blackbody as shown in Figure E.1. The blackbody temperature can then be determined from the peak intensity of an emission line. Since absolute intensity measurements are prone to error, fitting the blackbody curve to several separate optically thick peaks gives a more accurate result. The expression for the radiation intensity per unit wavelength per unit solid angle is[E.2]

$$I_o = \frac{2hc^2}{\lambda^5} \frac{1}{e^{hc/kT\lambda} - 1} \qquad (E.3)$$

where h is Planck's constant and c is the speed of light.

Perhaps the most useful application of thermal emission is to identify the presence of various species and obtain order of magnitude estimates of their concentrations. Since each species has unique spectral features, passing the collected light through a spectrometer will indicate what is present in the flow. A measurement of the relative concentration of these species is complicated by the different emission coefficients and optical quenching for an optically thin gas, and different emissivities and optical depth for an optically thick gas. Nevertheless, a general sense of the relative concentrations of various species can be had by comparing spectral line strengths. Hot luminous particles, of course, are always optically thick so their temperatures can be obtained by fitting their spectra to the blackbody distribution given in equation (E.3). Clearly due to the non-equilibrium effects, the particle's temperature will in general deviate from

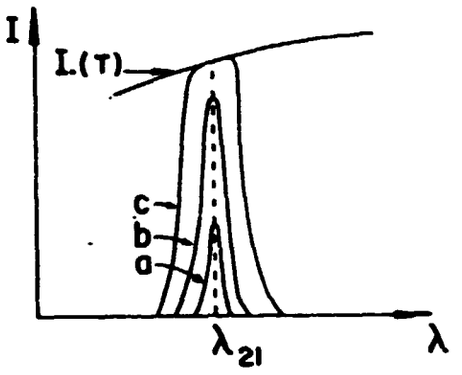

Figure E.1 An optically thick line approaches the blackbody radiation curve, $I_o(T)$. Curves a, b, and c represent emission from a spectral line with increasing optical thickness.

the gas temperature.

If there are few particles in the flow, particle velocities may also be measured using a time-of-flight technique.[E.4] Two points in the flow, separated by a known distance are focused onto different detectors. As a particle passes through, its emission is picked up by each detector sequentially giving two pulses whose times are separated by the time it took the particle to pass from the first region to the second. This, of course, assumes that the velocity vector of the particle is such that it actually passes through the two sample points.

Thermal emission must also be considered as a potential noise source for other measurements such as Rayleigh scattering, laser induced fluorescence, etc. It is therefore important to estimate to thermal emission intensity in order to determine what steps need be taken to eliminate it from these other measurements. An estimate begins with the radiative transfer equation,[E.5]

$$\frac{1}{c}\left(\frac{\partial I_\lambda}{\partial t} + \frac{c\partial I_\lambda}{\partial s'}\right) = J_\lambda \left(1 + \frac{\lambda^5}{2hc^2} I_\lambda\right) - K_\lambda I_\lambda \qquad (E.4)$$

where I_λ is the thermal emission intensity, s' is the displacement along a ray of light and J_λ and K_λ are the emission and absorption coefficients per unit wavelength, respectively. These coefficients may be related by invoking the law of detailed balance. That is, emission and absorption are related by the temperature since both must occur with equal probability at thermal equilibrium.

$$J_\lambda = \frac{K_\lambda e^{-hc/kT\lambda}}{2hc^2/\lambda^5} \qquad (E.5)$$

The radiative transfer equation at steady state then becomes

$$\frac{\partial I_\lambda}{\partial s'} = K'_\lambda (I_o - I_\lambda) \qquad (E.6)$$

where I_o is the blackbody intensity distribution from equation (E.2) and

$$K'_\lambda = K_\lambda (1 - e^{-hc/kT\lambda}) \tag{E.7}$$

This expression may be analytically integrated for the ideal case of a homogeneous radiating plane of finite thickness, d,[E.5]

$$I_\lambda(d) = I_o(1 - e^{-K'_\lambda d}) \tag{E.8}$$

A schematic of the detection configuration expected on a re-entry vehicle is shown in Figure E.2. The hot region between the shock and the wall is radiating. The high temperature region immediately downstream from the shock will be used to determine the absorption coefficient in equation (E.8). The luminous layer thickness, d, is assumed to extend from the shock to the plateau shown in Figure 1 in the main section of this report, and includes the region with a large temperature gradient. It is assumed, for simplicity, that the gas temperature and density is homogeneous in this layer. All the optical detection processes for which thermal emission is a potential noise source use a lens to collect the signal. The same lens will then also collect background light due to thermal emissions. This light is a distributed source and the total intensity may be found by integrating over the aperture to yield

$$I_{\lambda a} = \frac{\pi}{4} I_o \frac{\tau}{F^2} \Delta\lambda \tag{E.9}$$

where F is the f number of the collection optics (F = lens focal length/lens diameter), $\tau = K'_\lambda d$ is the optical depth (assumed to be $<<1$), and $\Delta\lambda$ is the bandwidth of the interference filter. The absorption coefficient per meter in hot air ($T < 20{,}000°K$) is taken from Zel'dovitch and Raizer,[E.4]

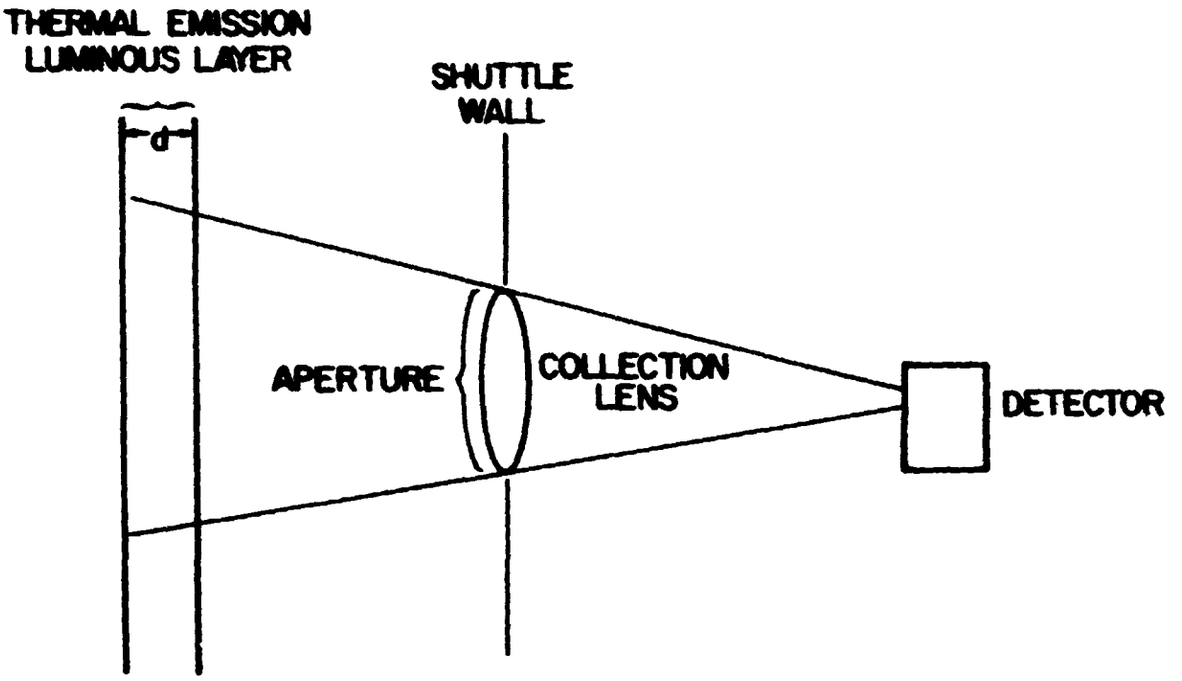

Figure E.2 Diagram of the optical collection system through which thermal emission will be collected. The lens is used for other experiments such as Rayleigh or Raman scattering.

$$K_\lambda = 8.6 \cdot 10^{19}\, \rho \cdot T \cdot \lambda^3\, e^{\frac{1.44 \cdot 10^{-2}}{\lambda \cdot T}} \left(C_{O_2}\, e^{\frac{-140{,}000}{T}} + C_{N_2}\, e^{\frac{-181{,}000}{T}} + C_O\, e^{\frac{-158{,}000}{T}} + C_N\, e^{\frac{-169{,}000}{T}} + C_{NO}\, e^{\frac{-108{,}000}{T}} \right) \qquad (E.10)$$

where ρ is the density in kg/m^3, T is in °K, λ is the wavelength in meters and C_i is the concentration of species i. K_λ and I_o have been plotted for different temperatures versus wavelength in Figures E.3 and E.4. The flow conditions assumed are taken from the simulation by J. L. Shinn, J. W. Moss, an· A. L. Simmonds of NASA Langley for a nonequilibrium flow, fully catalytic wall calculation at an altitude of 75 km and at a position along the surface of the Shuttle corresponding to 10 nose radii.

As an example, consider:

$d = 0.1$ m

$\lambda = 510$ nm (copper vapor laser)

$F = 10$

$T = 10^4$°K

$\Delta\lambda = 0.1 \times 10^{-9}$ m (state-of-the-art interference filter).

From Figures E.3 and E.4, $I_o = 2 \times 10^8$ $W/m^2\mu$ and $K_\lambda = 1.1 \times 10^{-4}$ m^{-1}. The optical depth, τ, is $1.1 \times 10^{-5} << 1$ and equation (E.9) may be used. The intensity radiated into the aperture is 2×10^{-3} W/m^2. By comparison the contribution to the intensity from thermal radiation in the flow at a temperature of 3000°K is negligible.

In summary, thermal emissions from gases have a potential for indicating gas temperatures and species identities. This will only be the case in the very high temperature region behind a high altitude shock. At lower altitudes, where the temperatures behind the shock are substantially less, the amount of fluorescence collected in the visible region of the spectrum is

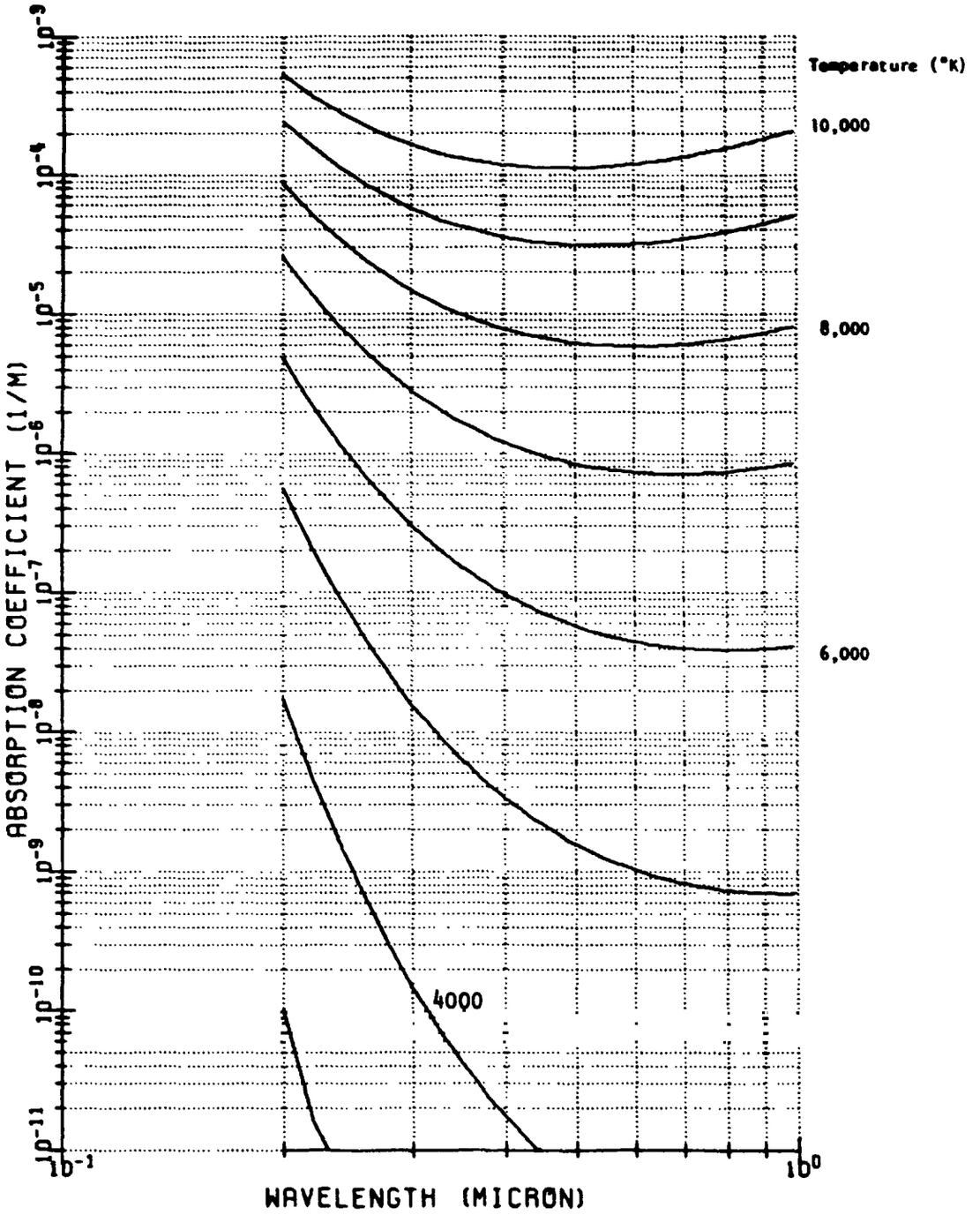

Figure E.3 Absorption coefficient (Equation E.10) versus wavelength for various temperatures. The flow conditions assumed are given by Moss's calculation for nonequilibrium flow, fully catalytic wall at an altitude of 75 km and $s/R_N = 10$.

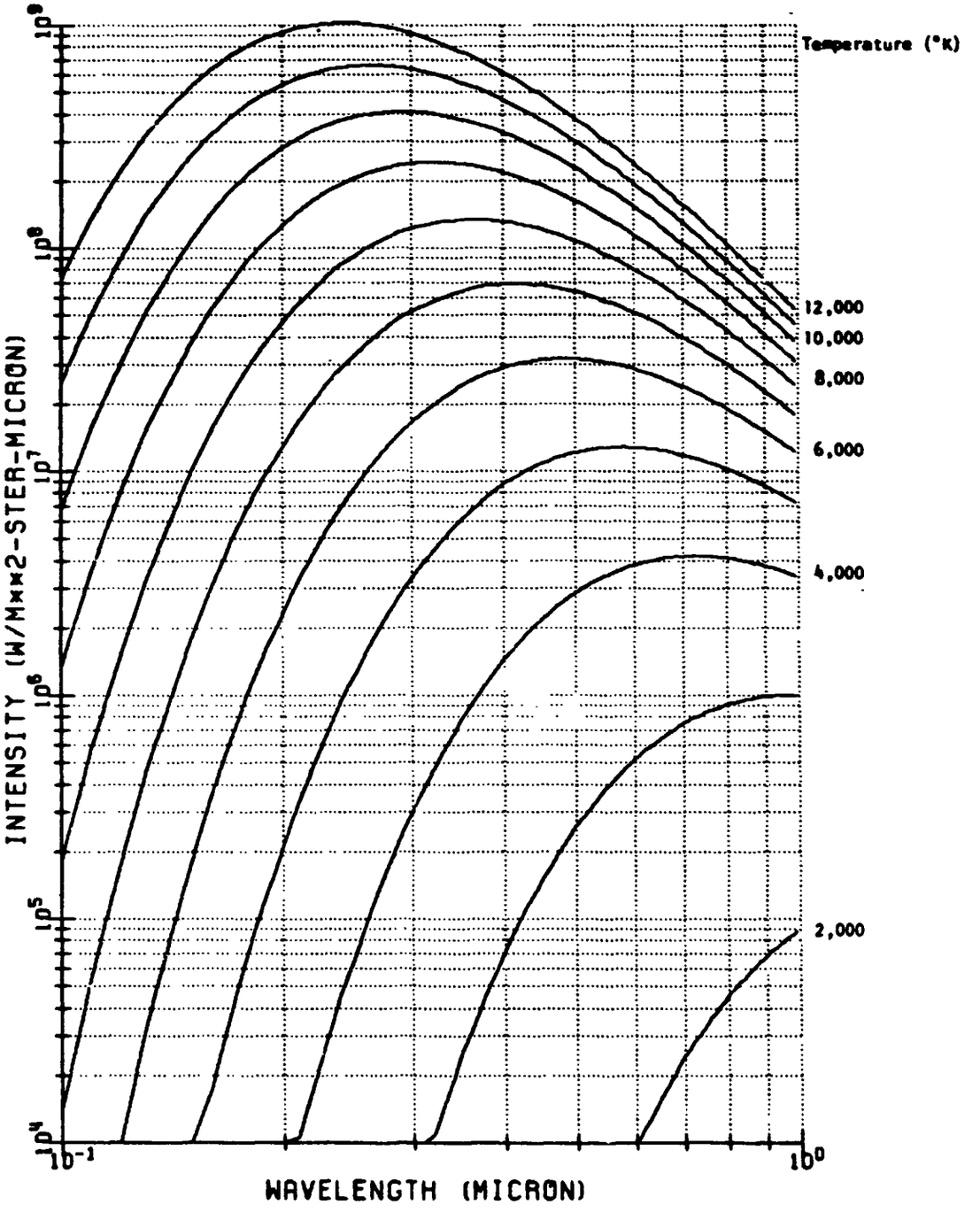

Figure E.4 Black-body radiation versus wavelength at different temperatures.

too low for meaningful diagnostics. Point measurements can only be made if the region behind the shock is assumed to be thin so no other molecules contribute to the signal between the observation port and the region of interest. Otherwise, the integrated path through fluorescing molecules makes point observations impossible. Additional uncertainty regarding the values of the quenching rates further complicates quantitative data analysis. In the high altitude region, however, thermal emission will certainly contain useful qualitative information on species identification.

The potential of thermal emissions as a noise background which would interfere with other optical measurements is most severe at high altitudes where fluorescence intensities are substantial. Early experiments should include a monitor for thermal emissions to both determine the utility of this technique for qualitative flow diagnostics as well as to establish its potential as a noise source for other optical measurements of interest. Since thermal emission is continuous in time, experiments seeking to eliminate thermal emission as a noise source can use pulsed lasers and signal gating to further suppress its effect. The importance of emission due to hot particles is difficult to assess since the density of particles in the flow has not been established. As is recommended elsewhere, early experiments should also seek to determine particle densities and sizes in order to further evaluate the possibility of using these particles for flow field measurements as well as their potential as a background noise source in other diagnostics.

References

E.1 Muntz, E. P., The electron beam fluorescence technique, AGARDograph 132, 1969.

E.2 Thorne, A. P., Spectrophysics (Chapman and Hall, London, 1974).

E.3 Generalov, N. A., Methods of Experimental Physics 18B, Emrich, R. J., editor (Academic Press, N.Y., 1981).

E.4 Trolinger, J. D. and Houser, M. J., Flight Dynamics Laboratory Technical Report AFWAL-TR-81-3080, 1981.

E.5 Zel'dovich, Y. B. and Raizer, Y. P., Physics of Shock Waves and High-Temperature Hydrodynamic Phenomena (Academic Press, New York and London, 1967).

APPENDIX F. ELECTRON-BEAM FLUORESCENCE

Symbol	Units	Description
A_{jk}	sec^{-1}	Einstein spontaneous emission coefficient for level j to k
I_{jk}	$watts/meter^2$	emission intensity from level j to level k
k	1.38054×10^{-23} joules/°K	Boltzmann's constant
m	Kg	mass
N_i	$meters^{-3}$	number density of species i
Q_{ij}	$meters^2$	quenching collision cross section of species i with species j
q(v',v'')		Franck Condon factor between levels v' and v''
U	meters/sec	flow velocity
$\bar{v}_{ij}$	meters/sec	relative velocity between species i and j
λ	meters	wavelength
ν	Hertz	radiation frequency
$\delta\nu_D$	Hertz	Doppler shift of resonant frequency
$\Delta\nu_G$	Hertz	thermal (Gaussian) spectral line width--full width at half maximum

TABLE F.1 List of Symbols.

The electron-beam fluorescence technique is currently used to measure the static, vibrational, rotational, and translational temperatures of low density gaseous flows as well as to determine gas species concentration and density, measure velocity, and provide flow visualization. Reviews of this technique have been written by E. P. Muntz,[F.1] and the present discussion draws heavily on these works.

A collimated beam of electrons of about 1 mm in diameter is directed into a flow, exciting the gas species into higher energy levels. These species fluoresce over a characteristic lifetime as they relax back to the unexcited state. An optical detector may be configured to monitor the fluorescence from any position along the beam to give a spatial resolution of ~ 1 mm^3. The resulting spectrum is characteristic of the composition, temperature, density, and velocity of the gas.[F.2,F.3] The many different parameters on which the electron-beam fluorescence is dependent make it an attractive technique. Its use is usually limited to number densities of less than 10^{16} cm^{-3}, though some investigators have extended the range to 10^{18} cm^{-3}.[F.4] The electron beam loses its collimation and penetration depth at higher densities, and the fluorescence is no longer linearly related to density. The technique has been applied in temperature ranges from a few degrees up to 1000°K.

Nitrogen and air flows have been the most extensively investigated. The major emission in both occurs for the first negative system of N_2^+ at 391.4 nm. A 50,000 electron volt beam exciting the first negative system of nitrogen with a 1 mA/mm^2 of current can produce 10^{11} photons per second depending on geometry and number density. The fluorescence provides a qualitative tool for visualizing the flow. Incomplete knowledge of quenching rates and Franck-Condon factors limits quantitative data interpretation.[F.1]

The most straightforward quantitative measurement is the nitrogen density. This measurement requires a density independent transfer of energy from the electrons to the nitrogen-excited state. There are several mechanisms for accomplishing this transfer: 1) Collision of nitrogen with primary high energy electrons originating from the electron beam; 2) Collision of nitrogen with secondary electrons produced by species ionization due to

collisions with primary electrons; 3) Absorption of electron beam generated photons by unexcited nitrogen molecules; 4) Energy transfer by collisions of nitrogen with other excited particles; 5) Transfer of energy to the excited state in a single molecule by cascade from higher electronic states in the same molecule. The excited state is subsequently depopulated by spontaneous emission and quenching collisions. The emission is observed as signal; the quenching collisions compete with the emission and reduce the signal.

If only the primary electrons are assumed to populate the excited state j, then the fluorescence emission to state k, I_{jk}, is related to the gas density, N_i, by[F.1]

$$I_{jk} = K N_i \frac{1}{1 + 2N_i \frac{Q_{ii} \bar{V}_{ii}}{A_{jk} + A_T}} \qquad (F.1)$$

where K is a constant, Q_{ii} is the quenching collision cross section, A_{jk} is the spontaneous emission for the transition $j \rightarrow k$, A_T is the spontaneous emission for all other transitions, and $\bar{V}_{ii}$ is the relative velocity between the molecules. At low density the emission, I_{jk}, is essentially proportional to the gas density. At densities higher than 10^{16}/cc the fluorescence intensity is strongly quenched and is no longer sensitive to density variations. Most density measurements are performed in the linear portion of the response curve. The accuracy of density measurement can approach ± 1 percent if the calibration procedure is carefully executed; however, ± 5 percent is more typical. The large number of fluorescent photons reduces photon statistical noise to a low level. Inaccuracies are introduced by the quenching process which is both species and temperature dependent.

Some experimental work has been conducted at higher densities[F.4] ($10^{16} \leq n \leq 10^{18}$ cm^{-3}). This is the nonlinear regime, and a careful calibration is required over the complete range of density and temperature.

In a nonequilibrium gas, the vibrational and rotational energy distributions may not be in equilibrium with each other or with the local temperature. For example, the vibrational levels may separately reach an equilibrium which may be described by a temperature but is different from the true translational temperature of the gas. To measure this vibrational temperature, first consider a ground electronic state molecule with vibrational level v_1'' excited to the v' vibrational state of the upper electronic level with subsequent decay to the v_2'' vibrational level of the ground electronic state. If only spontaneous emission depopulates the upper state and quenching is neglected, then the intensity of fluorescence is[F.1]

$$I_{v'v_2''} = K \nu^4_{v'v_2''} \frac{q(v',v_2'') \sum_{v_1''} N_{v_1''} q(v'v_1'')}{\sum_{v_2''} \nu^3_{v'v_2''} q(v'v_2'')} \qquad (F.2)$$

where K is a constant, ν is the frequency, n is the number density, and q is the Franck-Condon factor. The vibrational temperature information is contained explicitly in the number density, $N_{v_1''}$, which is assumed to follow a Boltzmann distribution. By monitoring the fluorescence intensity from two separable vibrational lines and taking their ratio, one may obtain a curve which is temperature sensitive and independent of the constant K.

The technique has been checked at low densities and up to 300°K with a resulting accuracy of ±10%.[F.5] Quenching invalidates equation (F.2) at higher densities. The number of vibrational levels involved in the calculation rises with temperature. This introduces an additional uncertainty because

of the larger number of Franck-Condon factors involved. Higher temperatures also have a bearing on the quenching process.

Similarly, the rotational modes may reach a separate "temperature." The expression which provides the rotational temperature is rather involved, requiring an iteration process and will therefore not be given here. Analagous difficulties to those associated with the vibrational temperature measurement are encountered with the rotational temperature measurement, and they are related to uncertainties in the knowledge of quenching rates and Franck-Condon factors. The rotational temperature can in many cases be assumed equal to the translational temperature; however, this is not always true for the vibrational temperature.

Low density is still a requirement to minimize quenching, but accuracies of better than $\pm 5°K$ have been achieved at temperatures below 1000°K.[F.6] Large discrepancies exist for temperatures below 300°K. Their origin is still unknown.

The translational temperature is considered to be the true local temperature. The translational temperature may be obtained by spectrally resolving the fluorescence emission of a particular transition. The instrument most frequently used in a Fabry-Perot interferometer. The line shape observed has a Gaussian component which is related to Doppler broadening because of the random motions of the molecules. The temperature of the flow, T, is related to the full width at half maximum, $\Delta\nu_G$, of the Gaussian line shape by[F.1]

$$T = \left(\frac{\Delta\nu_G \cdot \lambda_{21}}{2}\right)^2 \frac{m}{2k \ln 2} \qquad (F.3)$$

where λ_{21} is the wavelength of the transition, m is the mass of a single atom, and k is Boltzmann's constant. Under optimum conditions, the technique can

measure the translational temperature in helium with an accuracy of a few degrees K at room temperature. The accuracy in other gases depends on the fluorescence intensity and the ratio between the Doppler width and the collisional and instrumental widths.

Electron-beam fluorescence can be used for velocity measurements by observing the Doppler shift of the fluorescence. A comparison of the fluorescence spectrum of a stationary gas with the same transition in moving gas gives the Doppler shift, $\delta\nu_D$. The velocity, U, may then be calculated from[F.4]

$$U = \delta\nu_D \cdot \lambda \qquad (F.4)$$

where λ is the wavelength of the observed transition. The relative accuracy of the measurement depends on the relative size of the Doppler shift, $\delta\nu_D$, in comparison to the combined temperature collisional and instrumental broadening, $\Delta\nu$. A 'tracking' Fabry-Perot interferometer, locked to the spectral peak by phase sensitive detection simplifies velocity measurements, since it eliminates the need to scan the complete spectrum.

The fluorescence emission also provides a method for density sensitive flow visualization. Fluorescence in the close proximity to the electron beam is observed for N_2, O_2, and NO. An afterglow is obtained in He flows becuase of the excitation of a metastable state. Hence, in wind tunnels, the He gas fluoresces far downstream, but in air the electron beam has to pass through the position of interest.

The researchers contacted all agreed that the utility of the electron-beam technique is limited by insufficient knowledge of quenching rates which leads to large uncertainties in temperature measurements. It was felt by Professor Larry Talbot of the University of California-Berkeley and Dr. William Hunter of NASA Langley that electron-beam fluorescence was most

useful as a flow-visualization tool in wind tunnels. Dr. Robert Cattolica of Sandia-Livermore felt that it would be worthwhile to undertake measurements at very high altitudes. At high altitudes (somewhat above those of interest in this study), the densities will be low enough so that the data could be interpreted quantitatively. At lower altitudes, quenching will eliminate this possibility, but gross features of the flow may still be observable.

In summary, the electron-beam fluorescence technique is attractive because of the many properties which it can measure and because the signal is not limited by photon statistics noise. In the linear response region the instrument can only be used at the highest altitude of interest. At lower altitude, one could possibly apply it to density measurements only after careful calibration.

Major uncertainties in temperature measurements arise from insufficient knowledge of the quenching and Franck-Condon factors particularly at the high temperatures existing in the flow. Velocity measurements are best performed on atoms but have not been demonstrated on nitrogen or other species present in the flow. Since a fluorescence signal will also be present, it might be useful to use an electron beam at least for flow visualization and try to extract quantitative data by proper calibration at the higher altitudes.

References

F.1 Muntz, E. P., Methods of Experimental Physics, 18B. R.J. Emrich editor, (Academic Press, New York, 1981).
Muntz, E. P., The Electron Beam Fluorescence Technique, AGARDograph 132, 1969.

F.2 Hunter, W. W., Electron Beam Measurements of Rotational Temperature with Vibrational Temperature Greater than 800°K, AIAA J. 8, 959 (1970).

F.3 Becker, M., Robbens, F. and Cattolica, R., Velocity Distribution Functions Near the Leading Edge of a Flat Plate, AIAA J. 12, 1247 (1970).

F.4 Smith, J.A. and Driscoll, J.R., AGARD Conference Proceedings No. 193 on Applications of Non-Intrusive Instrumentation in Fluid Flow Research, AGARD CP-193 (Harford House, London, 1976), paper 16-1.

F.5 Langstroth, G.O., The excitation of Band Systems by Electron Impact, Roy. Soc. Lon.-Proc. 146, 166 (1934).
Fan, C.Y., Emission Spectra Excited by Electronic and Ionic Impact, Phys. Rev. 103, 1740 (1956).
Sheridan, J.R. and Clark, K.C., Vibration and Rotation of N_2^+ Excited by 10-65 keV Ions, Phys. Rev. 140, A1033 (1965).

F.6 Coe, D., Robben, F. and Talbot, L., in Rarified Gas Dynamics, R. Campargue editor, Abst. 160.C.E.A., Paris, 1978.
Karelov, N.V., Rebrov, A.K. and Sharafutdinov, R.G., in Rarified Gas Dynamics, R. Campargue editor, Abst. 135.C.E.A., Paris, 1978.

APPENDIX G. RAMAN SCATTERING

Symbol	Units	Description
h	6.6256×10^{-34} joule-sec	Planck's constant
L	meters	sample volume length
N_i	meters^{-3}	number density of scattering molecule in energy level i
n_p		number of pulses per measurement interval
P_{RAMAN}	watts	Raman scattered signal power
P_o	watts	incident laser power
$(S/N)_{RAMAN}$		Raman scattering signal to noise ratio
Δt	second	·ser pulse duration
η_C		.iciency of the collection optics
η_D		efficiency of the detector
λ	meters	laser wavelength
ν	Hertz	frequency of scattered radiation
$(\frac{d\sigma}{d\Omega})_{RAMAN}$	meter^2/ steradian-molecule	differential Raman scattering cross section
Ω_c	steradians	solid angle of collect.. optics

TABLE G.1 List of symbols.

Raman scattering is an inelastic scattering process where the wave number shift of the scattered light is characteristic of the spacing between the scattering molecule's rotational, vibrational, and electronic energy levels. Raman scattering can be used to measure the number density of the scattering species and the gas temperature.

For a specific rotational, vibrational, and electronic energy level transition, A→B, the Raman scattered signal strength, in terms of power, is given by the following expression

$$P_{RAMAN} = P_o N_i \left(\frac{d\sigma}{d\Omega}\right)_{RAMAN} L \Omega_c \eta_C \eta_D \qquad (G.1)$$

where P_o is the power of the incident laser beam, N_i is the number density of the scattering species in the initial state, $\left(\frac{d\sigma}{d\Omega}\right)_{RAMAN}$ is the differential Raman scattering cross-section, L is the length of the incident beam from which scattered light is collected, Ω_c is the solid angle of the collection optics, η_C is the efficiency of the collection optics, and η_D is the detector quantum efficiency.

The Raman scattered light corresponding to different energy level transitions is at different wavelengths, and its intensity is proporational to the population of the initial energy level of the particular transition. This results in a spectral shape which is a function of the relative population of the energy levels and can be related to the gas temperature under equilibrium conditions. The integrated spectrum in turn is proportional to the total number density of the scattering species.

The sensitivity and accuracy of Raman scattering for species density measurements was evaluated in terms of the minimum detectable species density for a given signal to noise ratio.[G.1] The noise was assumed to be quantum noise which is equal to the square root of the number of detected Raman photons; therefore, the signal to noise ratio is given by:

$$(S/N)_{RAMAN} = (P_{RAMAN} \Delta t \, n_p/h\nu)^{1/2} \qquad (G.2)$$

where Δt the pulse duration, n_p is the number of pulses during the measurement interval, h is Planck's constant, and ν is the radiation frequency.

In order to determine the minimum detectable number density for a given signal to noise ratio, the experimental parameters in equations (G.1) and (G.2) must be specified. The experimental parameters have been selected to give maximum signal strength and to be consistent with any constraints imposed by the proposed flow field measurements. The experimental parameters are summarized in Table G.2. A KrF laser and a copper vapor laser were considered for the Raman measurement. The KrF was considered because of its high average power (1 J/pulse at 25 Hz) and its UV output (249 nm) which results in larger Raman cross-section and in greater detector quantum efficiencies. The copper vapor laser was considered because of its high average power (10 mJ/pulse at 5000 Hz). The measurement length L is chosen to be 5 mm based on the spatial resolution required to characterize the boundary layer profiles which were predicted by the numerical computations.[G.2] It is assumed that for the density measurements the integrated Raman spectrum would be used, in which case N_i becomes the total number density of the scattering species. Based on the rate of descent of the Space Shuttle, an integration time up to 10 seconds was assumed to make the measurements because the state conditions do not vary rapidly. In Table G.3 are listed the five species which are expected in the boundary layer,[G.2] the Raman transition wavelength of each, the Raman cross-section of each, and the minimum detectable density for a signal to noise ratio of 10 for pumping with both the KrF and the copper vapor laser.

The detectability estimates given in Table G.3 can be compared to the calculated[G.1] species densities at different altitudes, which are also summarized in Table G.3, in order to determine the altitudes at which Raman scattering concentration measurements are possible. Based on these results

		KrF Laser*	Copper Vapor Laser**
Incident Laser Power in Sample Volume	P_o	6.25 MW	0.1 MW
Pulse Length	Δt	16 nsec	50 nsec
Repetition Rate	n_p	25/sec	5×10^3/sec
Wavelength	λ	249 nm	510 nm
Detector Quantum Efficiency	η_D	0.35	0.1
Collector Optics Efficiency	η_C	0.1	0.1
Optics Collection Angle	Ω_c	0.01 str	0.01 str
Scattering Length	L	5 mm	5 mm

* Lambda Physik Model EMG 201.

** Plasma Kinetics Model 751

TABLE G.2 Values used for Raman scattering signal to noise estimates.

Species	Raman Transition	$\frac{d\sigma}{d\Omega} / \frac{d\sigma}{d\Omega}\Big\|_{N_2}$ *	Minimum Detectable Density with S/N = 10		Maximum Density**	
			KrF	Copper Vapor	75 km	52 km
N_2	Vibrational 2332 cm^{-1}	1.0	4.3×10^{15}/cc	3.6×10^{16}/cc	3×10^{16}/cc	1×10^{17}/cc
O_2	Vibrational 1557 cm^{-1}	1.2	3.8×10^{15}/cc	3.2×10^{16}/cc	6×10^{15}/cc	2×10^{16}/cc
NO	Vibrational 1877 cm^{-1}	0.55	7.8×10^{15}/cc	6.9×10^{16}/cc	3×10^{15}/cc	1×10^{16}/cc
N	Not Applicable	---	----	----	----	----
O	Electronic*** 158 cm^{-1}, 226 cm^{-1}	1.26	3.7×10^{15}/cc	3.3×10^{16}/cc	6×10^{15}/cc	2×10^{16}/cc

* $\frac{d\sigma}{d\Omega}\Big|_{N_2} = 4.4 \times 10^{-31}$ cm^2/steradian-molecule with 5145Å laser.[G.3]

** Reference G.2.

*** Reference G.4.

TABLE G.3 Minimum detectable density by Raman scattering compared with expected maximum densities at 75 km and 52 km altitudes.

and the requirement of a dynamic range of 10, using the KrF laser, N_2 can be measured at all altitudes up to 75 km, while O_2 and O can be measured at altitudes up to 52 km and NO cannot be measured; whereas with the copper vapor laser, N_2 can be measured at altitudes up to 52 km while O_2, NO, and O cannot be measured. It is important to re-emphasize that these detection estimates are made assuming no appreciable background noise from particulates (i.e. scattering or incandescence) or thermal emission.

The calculations[G.2] predict that the nitrogen mass fraction varies by less than 30% across the boundary layer profile for a given altitude and distance along the vehicle. If high accuracy and resolution measurements were available, the nitrogen density would indicate the status of the boundary layer and would act as benchmark data for computational codes. The total gas density changes by approximately a factor of 10 over a given boundary layer profile, therefore, a nitrogen density measurement could more easily be used as a measure of the total gas density.

For temperature measurements, one should use the most populous species, if possible, which in this case would be nitrogen. As shown above, using a KrF laser the detection of total N_2 concentration is possible at all altitudes. However, if one chooses to resolve the Q-branch spectrum for the purpose of curve fitting to determine the temperature, the partitioning of the signal among the different vibrational-rotational levels will increase the minimum N_2 density at which the thermometry measurements can be made by a factor of 100. In this case thermometry measurements would only be possible below 52 km. If a vibrational band ratio or Stokes/anti-Stokes approach is used for larger signal strengths, then the partition factor is in the worst case 10, and thermometry measurements can be made at all altitudes. This method, however, is subject to rather large errors. For example, one

would have to be concerned, especially near the shock, about non-equilibrium effects. The measured vibrational temperature may not be in equilibrium with the gas kinetic temperature. Thermal emission and laser induced fluorescence from particles will also lead to interpretation errors.

Another possibility for enhanced signal strengths would be to use resonance Raman scattering from O_2 (193 nm) or NO (220 nm) whereby several orders of magnitude greater signal strengths could be realized. As pointed out by Dr. Alan Eckbreth of United Technologies, this would require the use of a laser with excellent frequency stability. There are, however, no reports in the literature of resonance Raman measurements of O_2 or NO. Therefore little more can be concluded at this time.

The concensus of the researchers we interviewed was generally not as optimistic as these results. However, most of their concerns were related to the potential problem of background noise from particulates and thermal emission. There was agreement that characterization of these potential noise sources must be done before the final experiment selection and design is completed. Because of the weak signals associated with spontaneous Raman scattering, there was also agreement that fluorescence and Rayleigh measurements should be given more serious consideration.

References

G.1 Rahn, L.A., Mattern, P.L. and Farrow, R.L., 1981, "A Comparison of Coherent and Spontaneous Raman and Combustion Diagnostics," Eighteenth Symposium (International) on Combustion.

G.2 Shinn, J.L., Moss, J.N. and Simmonds, A.L., 1982, "Viscous-Shock-Layer Laminar Heating Analysis for the Shuttle Windward-Symmetry Plane with Surface Finite Catalytic Recombination Rates," AIAA/ASME Joint Fluids, Plasmas, Thermophysics and Heat Transfer Conference, June 7-11, 1982, St. Louis, Missouri.

G.3 Fouche, D.G. and Chang, R.K., 1971, "Relative Raman Cross Section for N_2, O_2, CO, CO_2, SO_2 and H_2S," Applied Physics Letters 18, 579.

G.4 Dasch, C.J. and Bechtel, J.H., 1981, "Spontaneous Raman Scattering by Ground State Oxygen Atoms," Optics Letters 6, 36.

APPENDIX H. COHERENT ANTI-STOKES RAMAN SCATTERING

Symbol	Units	Description
c	meters/sec	speed of light in vacuum
D	meters	laser beam diameter between $1/e^2$ intensity points
h	6.6256×10^{-34} joule-second	Planck's constant
$\hbar$	1.0545×10^{-34} joule-second	Planck's constant/2π
I_{AS}	watts/meter^2	intensity of coherent anti-Stokes Raman signal
I_P	watts/meter^2	intensity of pump laser
I_S	watts/meter^2	intensity of probe (Stokes) laser
Δj		fractional population difference between transition levels
N_i	meters^{-3}	total species number density of species i
n_p		number of pulses per measurement interval
P_{AS}	watts	coherent anti-Stokes Raman signal power
P_S	watts	power of probe (Stokes) laser
$(S/N)_{CARS}$		signal to noise ratio for coherent anti-Stokes Raman spectroscopy
Δt	seconds	laser pulse duration
z	meters	interaction length
γ	radians/sec	Raman line width
η		combined collection and detection efficiency
λ_{AS}	meters	anti-Stokes wavelength
λ_P	meters	pump laser wavelength
λ_S	meters	probe (Stokes) laser wavelength
ν	Hertz	radiation frequency

Symbol	Units	Description
$(\frac{d\sigma}{d\Omega})_{RAMAN}$	meter^2/ steradian-molecule	differential Raman scattering cross section
χ	meter^3/joule	nonlinear susceptibility
χ_{NR}	meter^3/joule	non-resonant part of nonlinear susceptibility
χ_R	meter^3/joule	resonant part of nonlinear susceptibility
$\Delta\omega$	radians/sec	Raman transition frequency
ω_{AS}	radians/sec	coherent anti-Stokes Raman frequency
ω_P	radians/sec	pump laser frequency
ω_S	radians/sec	probe (Stokes) laser frequency

TABLE H.1 List of Symbols.

Coherent anti-Stokes Raman scattering (CARS) is a three-photon, inelastic-scattering process which is enhanced as the difference in frequency between two incident laser beams nears resonance with an energy level transition of the scattering molecule. The scattered radiation is then at the Raman anti-Stokes wavelength. The intensity of the CARS signal, I_{AS}, at frequency ω_{AS} is given by the following equation.[H.1,H.2]

$$I_{AS} = \left(\frac{4\pi^2\omega_{AS}}{c}\right)^2 I_P^2 I_S |\chi|^2 z^2 \eta \qquad (H.1)$$

where

$$\omega_{AS} = 2\omega_P - \omega_S .$$

$$\chi = \chi_R + \chi_{NR}$$

and

$$\chi_R = \frac{2N_i c^4}{\hbar \omega_S^2} \left(\frac{d\sigma}{d\Omega}\right)_{RAMAN} \frac{\Delta\omega \, \Delta_J}{[\Delta\omega - (\omega_P - \omega_S)]^2 - i\gamma(\omega_P - \omega_S)} = \chi_R' + i\chi_R''$$

I_p is the intensity of the probe beam at frequency ω_P, I_S is the intensity of the Stokes beam at frequency ω_S, χ is the third-order nonlinear susceptibility

z is the distance over which the beams interact, c is the speed of light, and η is the combined interaction-collection-detection efficiency. The third-order susceptibility is composed of a resonant part, χ_R, and a non-resonant part, χ_{NR}. The resonant part of the third order susceptibility is dependent on N_i, the total species number density, $(\frac{d\sigma}{d\Omega})_{RAMAN}$, the Raman cross-section for the transition characterized by the frequency difference $\Delta\omega$, γ, the Raman line width, Δ_J, the fractional population difference between the levels in the transition, and $\hbar$, Planck's constant divided by 2π.

The CARS process is nonlinear in incident beam intensity, number density, and interaction length; whereas spontaneous scattering is linear in these parameters. Because of this nonlinear behavior for a given experimental situation, the CARS signal strength can be larger or smaller than the corresponding spontaneous Raman signal, depending on the number density. The CARS process must also satisfy a phase-matching requirement (i.e. conservation of momentum). Phase matching is possible with one-sided optical access; however, a wide-angle crossed-beam configuration must be used. This results in a shortened interaction length and limited traversing capability.

In order to estimate the CARS signal strength, one can assume that the Stokes and anti-Stokes beams have the same diameter. Equation (H.1) can then be written in terms of the CARS power

$$P_{AS} = \left(\frac{4\pi^2\omega_{AS}}{c^2}\right)^2 |\chi|^2 I_P^2 P_S z^2 \eta \qquad (H.2)$$

There are two limiting cases to consider when estimating the minimum detection limits. One case is the detection of a major species for which $\chi_R > \chi_{NR}$, and the other is the detection of a minor species for which $\chi_R < \chi_{NR}$. We will consider the measurements to be quantum noise limited in both cases. In the former case, the greatest source of noise is the quantum

noise in the signal itself, therefore

$$(S/N)_{CAPS} = \left(\frac{P_{AS}\,\Delta t\, n_p}{h\nu}\right)^{1/2} \qquad (H.3)$$

where $$|\chi|^2 = \chi_R'^2 + \chi_R''^2$$

In the latter case, the major noise source is the quantum noise in the nonresonant background. Therefore, the signal is the contribution due to $2\chi_R'\chi_{NR}$, and the noise is the square root of the contribution due to χ_{NR}^2. The ratio of these two reduces to equation (H.3), where $|\chi|^2 = 4\chi_R'^2$ is used in equation (H.2). Therefore, the difference in the detection limit for the major species and the minor species cases differs only by approximately a factor of two.

The minimum detectable nitrogen density for a signal-to-noise ratio of 10 can now be determined using equations (H.2) and (H.3). The assumed experimental parameters are listed in Table H.2. The resultant detectability limit is $10^{15}/cm^3$. This estimate is for 1500°K, whereas, away from the surface the temperatures are expected to be much higher. As the temperature increases, the rotational population spreads out over many more levels. The CARS strength is consequently reduced through the Δ_J term in the third order susceptibility. As Eckbreth pointed out, the contribution of adjacent lines will also be less at high temperature, further reducing the CARS strength.

If this result is compared with the calculated densities of N_2, O_2, NO, and O at different altitudes, N_2 can be detected at all altitudes; and O_2, NO, and O can be detected at 52 km and below. Again, the sensitivity will be less in the hotter regions away from the surface. In order to relate the CARS signal strength to the density, the gas temperature must be known, unless a particular transition can be selected for which the population

Pump laser wavelength		λ_p = 532 nm
Probe (Stokes) laser wavelength		λ_S = 607 nm
Anti-Stokes wavelength		λ_{AS} = 480 nm
Pump laser peak power		P_p = 10 MW
Probe (Stokes) laser peak power		P_S = 1 MW
Nonlinear susceptibility	$\chi_R = 3.2 \times 10^{-17}$ cm^3/erg at 1 atm, 1500°K*	
Combined efficiency		η = 0.01
Focused beam diameter		D = 200 μm
Pulse duration		Δt = 10 nsec
Number of pulses per measurement interval		n_p = 100
Interaction length (crossed-beam phase matching)		z = 100 μm

* Reference H.1.

TABLE H.2 Values used for CARS signal to noise estimates.

difference term is temperature independent. Determination of the temperature from the N_2 CARS spectrum requires resolving the spectrum which increases the minimum detection limits to $10^{17}/cm^3$ because of reduced χ_R away from the peak and the necessity to use broad-band CARS. Thermometry measurements therefore will only be possible at the lowest altitudes.

Because the detection limit analysis predicts adequate sensitivity at only the lowest altitudes and because of the severe limitation due to one-sided optical access, CARS is not viable for the proposed re-entry vehicle measurements. Several of the researchers interviewed have had extensive experience using CARS diagnostics and their comments were in general agreement with this conclusion.

References

H.1 Tolles, W.M. and Turner, R.D., 1977, "A Comparative Analysis of the Analytical Capabilities of Coherent Anti-Stokes Raman Spectroscopy (CARS) Relative to Raman Scattering and Absorption Spectroscopy," Applied Spectroscopy 31, 96.

H.2 Rahn, L.A., Mattern, P.L. and Farrow, R.L., 1981, "A Comparison of Coherent and Spontaneous Raman and Combustion Diagnostics," Eighteenth Symposium (International) on Combustion.

APPENDIX I. LASER DOPPLER VELOCIMETER

Symbol	Units	Description
ℓ	meters	length of the laser Doppler velocimeter fringe region
U_1	meters/sec	particle velocity
w	meters	width of the laser Doppler velocimeter fringe region
x_f	meters	distance between interference fringes
β	degrees	intersection angle of lasers for laser Doppler velocimetry
λ_o	meters	laser wavelength
$\Delta\nu$	Hertz	spectral linewidth--full width at half maximum
ν_B	Hertz	beat frequency produced by particle passing through the fringe pattern in laser Doppler velocimetry
$\Delta\nu_o$	Hertz	free spectral range of the Fabry-Perot interferometer

TABLE I.1 List of Symbols.

The laser Doppler velocimeter is useful for measuring fluid velocities. Laser light scattered by a particle moving with the flow experiences a Doppler frequency shift proportional to the velocity of the particle. A measurement of the shift in frequency then gives the particle velocity. The most commonly employed configuration uses two laser beams crossed in the sample region to produce interference fringes (Figure I.1). As the particle traverses this region, it crosses the fringes (Figure I.2) at a rate determined by the velocity, resulting in scattered light which is modulated at the crossing frequency. Spatial resolution is defined by either the beam-crossing volume or the collection optics with submillimeter resolution easily

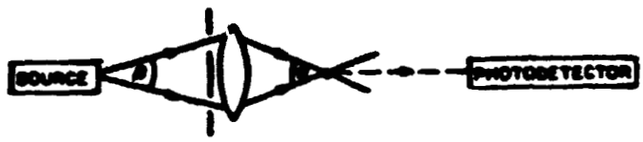

Figure 1.1 A laser Doppler velocimeter heterodyne detection configuration.

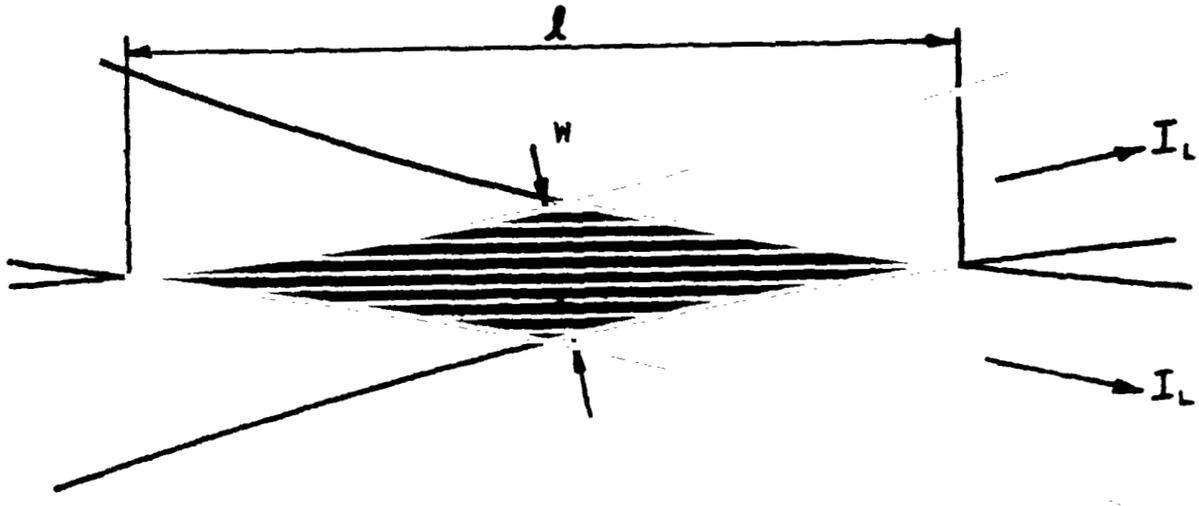

Figure 1.2 The fringe pattern created by two intersecting laser beams showing the interaction length ℓ and the width of the fringe region, w.

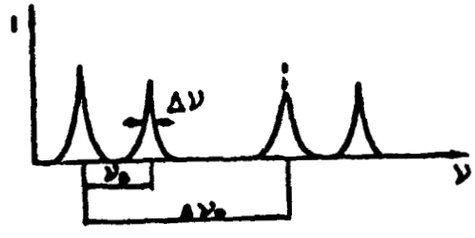

Figure 1.3 Fabry Perot output looking at light scattered off particles illuminated by two laser beams.

obtainable. A second approach employing a Fabry-Perot interferometer may be useful at high fluid velocities.[1.1] The laser Doppler velocimeter is non-intrusive and insensitive to other fluctuating flow parameters such as density and temperature. Velocity ranges from 10^{-3} cm/sec to 10^{6} m/sec have been measured. The difficulties associated with the use of the laser Doppler velocimeter are primarily because the flow has to be seeded and the particles do not track the flow in regions of high acceleration or low density.

The distance between the interference fringes, x_f, may be found from equation 1.1[1.1]

$$x_f = \frac{U_1}{\nu_B} = \frac{\lambda_o}{2 \sin \beta/2} \tag{1.1}$$

Here U_1 is the particle velocity in the plane of the two laser beams and perpendicular to their bisector, β is the intersection angle, λ_o is the laser wavelength, and ν_B is the beat frequency produced. The product of the output of the frequency counter, ν_B, and the fri. ge spacing, x_f, equals the velocity. Commercial laser Doppler velocimeter units can handle counting rates up to 200 MHz. State-of-the-art counters can go as high as 1 GHz which is also approximately the largest bandwidth of available photomultipliers. Counter and photomultiplier availability is therefore the limiting factor as far as high velocity measurements are concerned. Table 1.2 lists the counting frequencies, ν_B, for different beam intersecting angles, β, for an argon laser operating on the λ_o = 514.5 nm line and a particle velocity of U_1 = 5000 m/sec. From the table it is clear that the smaller the angle the more manageable the counting rate. If this method is to be used with a re-entry vehicle, very small angles will be required. An alternative approach to reduce the counting rate is to shift the frequency of one of the laser beams so the fringes scan in the direction of motion. This eliminates part of the

$\beta°$	x_f (μm)	ν_B (MHz)
45	0.7	7000
20	1.5	3333
5	6.0	835
1	30	166

TABLE I.2 Fringe spacing and counting frequencies for 514.5 nm laser beams intersecting at angle β and 5000 m/sec particles.

Doppler shift and is useful only if a narrow range of velocities are to be measured. A large value of interaction length permits the focusing of several detectors at different positions along the interacting volume to obtain a velocity profile. Clearly, the shallower the angle β, the longer the interaction length becomes.

The second approach circumvents the high counting rate problem by resolving the scattered light spectrally. A Fabry-Perot etalon is inserted between the intersecting volume and the detector. Two peaks are registered by the detector as the etalon is scanned as shown in Figure I.3. They correspond to the Doppler downshifted and upshifted light scattered by the two laser beams off the moving particles. The frequency difference between the two peaks is ν_B in equation (I.1). The value $\Delta\nu_o$ is the free spectral range of the Fabry-Perot etalon which provides a frequency calibration. While an upper bound limits the velocity measureable with the optical mixing configuration, a lower bound exists if the scattered light is to be spectrally resolved. When both scattered signals are put through the same etalon, the minimum measured velocity is limited by the Rayleigh criterion. A shift is

measureable only if it is larger than the width of the spectral line, $\Delta\nu \leq \nu_B$; otherwise, the two peaks coalesce. To overcome the limitation, a reference beam configuration may be employed whereby just one beam interrogates the flow while the other beam is used as a frequency reference. The scattered light from the flow and the reference beam are now directed into different etalons so that the peaks cannot overlap at small velocities. A single etalon may be employed if the frequency of the reference beam is shifted using a Bragg cell.

Two additional techniques which have been used and are related to laser Doppler velocimetry should be mentioned. One is the time-of-flight velocimeter[1,2] which may be used if the flow direction is known. Two parallel laser beams are ditected into the flow. A detector monitors the light pulses scattered off the particles as they pass through the beams. The velocity is deduced from the known separation of the beams and the time difference between the light pulses.

In a related technique discussed by Dr. Don Holve of Sandia Laboratories, the pulse shape of a particle traversing a single laser beam is resolved temporally and is independent of the particle size or trajectory. The time between two fractional values of the peak amplitude is related to the particle's velocity. The intensity of the pulses can also be used to obtain the particle size distribution; however velocity-size correlations cannot be determined.[1,2]

Two extensions of the LDV technique were mentioned in our meeting at Sandia. In the first, a holographic lens is employed to prolong the fringe pattern for multiple point measurements. The second is a time-of-flight measurement which takes advantage of gas breakdown by laser focusing. The

emitting plasma follows the flow and is monitored by two detectors which furnish the elapsed time.

The seeding problem poses the greatest difficulty as far as applying the LDV to measurements on board a re-entry vehicle. Particles injected through the wall of the craft may tend to stay close to the wall. Naturally occurring seed may be present or emitted from the ceramic cover of the re-entry vehicle, and these could be used for LDV measurements. The interference fringe detection schemes are more prevalent and easier to use. A very narrow angle β will be required to reduce the count frequency, but this also has the advantage of permitting multiple point measurements.

Thermally excited fluorescence emission and particulate luminosity may mask the signal. For these reasons it seems advisable as a first step to monitor fluorescence and particulate emission. This may be augmented by a laser to determine whether particles exist in the flow. Only after the environmental effects have been determined should an LDF measurement be attempted.

References

I.1 Somerscales, E.F.C., 1981, Methods of Experimental Physics, 18A, Emrich, R.J., editor (Academic Press, New York).

I.2 Schodl, R., 1977, Laser Two Focus Velocimetry (L2F) for Use in Aero Engines, in Laser Optical Measurement Methods for Aero Engine Research and Development, Weyer, H.B., Editor, AGARD Lecture Series No. 90.

I.3 Hurleman, D.E., 1978, Laser Technique for Simultaneous Particle-Size and -Velocity Measurements, Optics Letters 3, 19.

APPENDIX J. RESONANT DOPPLER VELOCIMETER

Symbol	Units	Description
c	meters/second	speed of light in vacuum
k	1.38054×10^{-23} joules/°K	Boltzmann's constant
$\hat{k}$		unit vector in the direction of laser propagation
m	Kg	mass
N	meters^{-3}	total species number density
T	°K	temperature
$\vec{U}$	meters/second	flow velocity vector
$\vec{u}$	meters/second	relative velocity
λ_{21}	meters	absorption wavelength of the particular species
$\delta\nu_D$	Hertz	Doppler shift of resonant frequency
$\Delta\nu_G$	Hertz	thermal (Gaussian) spectral linewidth--full width at half maximum
$\Delta\nu_L$	Hertz	Lorentzian spectral linewidth--full width at half maximum
ν_o	Hertz	absorption frequency
σ	meters^2	collision cross section

TABLE J.1 List of Symbols.

The Resonant Doppler Velocimeter (RDV)[J.1] has been used for visualization and for quantitative measurements of velocity, temperature, and density of a gaseous flow. These are achieved by shining a single frequency laser beam into a flow which is seeded with a selected atomic or molecular species. The laser is tuned through the absorption frequency of the seeded species

and the related resonance fluorescence is observed. An optical detector may be configured to monitor this fluorescence from any position along the beam to provide good spatial resolution. The velocity is determined by observing the Doppler shift of the absorption frequency. Spectroscopic absorption line broadening mechanisms furnish information regarding the static temperature and density of the moving gas.

The technique has been demonstrated in supersonic and hypersonic wind-tunnel flows. Unlike particles needed for the standard laser Doppler velocimeter, tracer atoms injected into the flow follow it closely. But the flow still has to be seeded, a fact which could raise experimental difficulties.

The velocity of the flow is measured by the Doppler shift $\delta\nu_D$ of the absorption line

$$\delta\nu_D = \nu_o \hat{k} \cdot \frac{\vec{U}}{c} \qquad (J.1)$$

where ν_o is the absorption frequency in the atomic rest frame, $\hat{k}$ is a unit vecto[illegible]irection of the laser beam, $\vec{U}$ is the flow velocity vector, and c [illegible]d of light. The method measures the velocity vector in the direction of the laser beam. A reference has to be furnished to be able to measure the absorption frequency in the atomic rest frame. This can be provided by performing spectroscopy in a stationary gas in a cell or in an atomic beam device.

The temperature and density of the flow give rise to frequency broadening of the spectral line. The temperature effect resul[illegible] in a line shape which is a Gaussian and the collision frequency, which is directly proportional to density, causes a Lorentzian line shape. Their combination is a convolution which is known as the Voigt profile. The observed profi[illegible] may be deconvolved to furnish the separate broadening components. The temperature

T, of the flow is given by

$$T = \left(\frac{\Delta\nu_G \lambda_{21}}{2}\right)^2 \frac{m}{2k \ln 2} \qquad (J.2)$$

where $\Delta\nu_G$ is the full width at the half maximum intensity points of the Gaussian line shape, λ_{21} and m are the absorption wavelength and mass of the particular species, respectively, and k is Boltzmann's constant. The density of the gas, N, is given by

$$N = \frac{\pi \Delta\nu_L}{\sigma \bar{u}} \qquad (J.3)$$

where $\Delta\nu_L$ is the full width at half maximum of the Lorentzian line shape, σ is the collision cross section, and $\bar{u}$ is the relative velocity in the center of mass system of the tracer atom and its colliding partner. The parameter σ is temperature independent if the hard sphere potential is used. In practice, the temperature dependence of σ must be determined by performing a calibration.[J.2]

The resonant Doppler velocimeter may also be used for flow-field visualization. Regions of higher density in the flow fluoresce brighter. In addition, by tuning the laser to a particular Doppler shifted absorption frequency, one can highlight the portions of the flow field which correspond to a particular velocity.

The many properties which can be measured by using the resonant Doppler velocimeter make it an attractive technique. The major difficulty lies in identifying the proper tracer atoms and seeding it into the flow. Sodium atoms have been used in nitrogen and helium flows, but sodium would tend to react with the atmospheric oxygen in the flow field surrounding the vehicle. Sodium does occur naturally in the atmosphere. At the highest altitude of interest (80 km), its concentration of 10^2 cm^{-3} is four orders of magnitude

below that used in the laboratory. At lower altitudes, its concentration is negligible, and the fluorescence signal will be masked by Rayleigh scattering.

Laser-induced fluorescence has been demonstrated on N, O, and NO suggesting that they could be used as tracers for applying the resonant Doppler velocimeter. The major difficulty is associated with producing a tunable laser system with a narrow linewidth and an output frequency which matches one of the ultraviolet absorption frequencies of the gases present.

References

J.1 Zimmermann, M. and Miles, R.B., 1980, Hypersonic-Helium-Flow-Field Measurements with the Resonant Doppler Velocimeter, Applied Physics Letters 37, 885.

J.2 Zimmermann, M. and Miles, R.B., 1981, Low Temperature He-Na Collision Rate Measurements, Journal of Physics B: At. Mol. Phys. 14, L85.